

# A decentralized scalable approach to voltage control of DC islanded microgrids

Michele Tucci<sup>\*1</sup>, Stefano Riverso<sup>†2</sup>, Juan C. Vasquez<sup>‡ 3</sup>, Josep M. Guerrero<sup>§ 3</sup>, and Giancarlo Ferrari-Trecate<sup>¶ 1</sup>

<sup>1</sup>*Dipartimento di Ingegneria Industriale e dell'Informazione, Università degli Studi di Pavia*

<sup>2</sup>*United Technologies Research Center Ireland*

<sup>3</sup>*Institute of Energy Technology, Aalborg University*

**Technical Report**  
March, 2015

## Abstract

We propose a new decentralized control scheme for DC Islanded microGrids (ImGs) composed by several Distributed Generation Units (DGUs) with a general interconnection topology. Each local controller regulates to a reference value the voltage of the Point of Common Coupling (PCC) of the corresponding DGU. Notably, off-line control design is conducted in a Plug-and-Play (PnP) fashion meaning that (i) the possibility of adding/removing a DGU without spoiling stability of the overall ImG is checked through an optimization problem; (ii) when a DGU is plugged in or out at most neighbouring DGUs have to update their controllers and (iii) the synthesis of a local controller uses only information on the corresponding DGU and lines connected to it. This guarantee total scalability of control synthesis as the ImG size grows or DGU gets replaced. Yes, under mild approximations of line dynamics, we formally guarantee stability of the overall closed-loop ImG. The performance of the proposed controllers is analyzed simulating different scenarios in PSCAD.

*Keywords:* Decentralized control, plug-and-play, DC microgrid, islanded microgrid, voltage control.

---

<sup>\*</sup>Electronic address: [michele.tucci02@universitadipavia.it](mailto:michele.tucci02@universitadipavia.it); Corresponding author

<sup>†</sup>Electronic address: [riverss@utrc.com](mailto:riverss@utrc.com)

<sup>‡</sup>Electronic address: [joz@et.aau.dk](mailto:joz@et.aau.dk)

<sup>§</sup>Electronic address: [juq@et.aau.dk](mailto:juq@et.aau.dk)

<sup>¶</sup>Electronic address: [giancarlo.ferrari@unipv.it](mailto:giancarlo.ferrari@unipv.it)

# 1 Introduction

In the recent years, the increasing penetration of renewable energy sources has motivated a growing interest for microgrids, energy networks composed by the interconnection of DGUs and loads [1]. Microgrids are self-sustained electric systems that can supply local loads even in islanded mode, i.e. disconnected from the main grid [2]. Besides their use for electrifying remote areas, islands, or large buildings, microgrids can be used for improving resilience to faults and power quality in power networks [3]. So far, research mainly focused on AC microgrids [1, 2, 3, 4, 5]. However, technological advances in power electronics converters have considerably facilitated the operation of DC power systems. This, together with the increasing use of DC renewables (e.g. PV panels), batteries and loads (e.g. electronic appliances, LEDs and electric vehicles), has triggered a major interest in DC microgrids [6, 7, 8]. DC microgrids have also several advantages over their AC counterparts. For instance, control of reactive power or unbalanced electric signals are not an issue. On the other hand, protection of DC systems is still a challenging problem [8].

For AC ImGs a key issue is to guarantee voltage and frequency stability by controlling inverters interfacing energy sources with lines and loads. This problem has received great attention and several decentralized control schemes have been proposed, ranging from classic droop control [2, 9], to decentralized control [10, 4, 5]. Some control design approaches are scalable, meaning that the design of a local controller for a DGU is not based on the knowledge of the whole ImG and the complexity of local control design is independent of the ImG size. In addition, the method proposed in [4, 5] allows for the seamless plugging-in, unplugging and replacement of DGUs without spoiling ImG stability. Control design procedure with these features have been termed PnP [11, 12, 13, 14].

Voltage stability is critical also in DC microgrids as they cannot be directly coupled to an “infinite-power” source, such as the AC main grid, and therefore they always operate in islanded mode. Existing controllers for the stabilization of DC ImGs are mainly based on droop control [7, 15]. So far, however, stability of the closed-loop systems has been analyzed only for specific ImGs [7, 15].

In this paper we develop a totally scalable method for the synthesis of decentralized controllers for DC ImGs. We propose a PnP design procedure where the synthesis of a local controller requires only the model of the corresponding DGU and the parameters of transmission lines connected to it. Importantly, no specific information about any other DGU is needed. Moreover, when a DGU is plugged in or out, only DGUs physically connected to it have to retune their local controllers. As in [4], we exploit Quasi-Stationary Line (QSL) approximations of line dynamics [16] and use structured Lyapunov functions for mapping control design into a Linear Matrix Inequality (LMI) problem. This also allows to automatically deny plugging-in/out requests if these operations spoil the stability of the ImG.

In order to validate our results, we run several simulations in PSCAD using realistic models of Buck converters and associated filters. As a first test, we consider two radially connected DGUs [17] and we show that, in spite of QSL approximations, PnP controllers lead to very good performances in terms of voltage tracking and robustness to unknown load dynamics. We also show how to embed PnP controllers in a bumpless transfer scheme [18] so as to avoid abrupt changes of the control variables due to controller switching. Then, we consider an ImG with 5 DGUs arranged in a meshed topology including loops and discuss the real-time plugging-in and out of a DGU.

The paper is organized as follows. In Section 2 we present dynamical models of ImGs and the adopted line approximation. In Section 3, the procedure for performing PnP operations is described. In Section 4 we assess performance of PnP controllers through simulation case studies. Section 5 is devoted to some conclusions.

## 2 Model of a DC Microgrid

This section discusses dynamic models of ImGs. For clarity, we start by introducing an ImG consisting of two parallel DGUs, then we generalize the model to ImGs composed of  $N$  DGUs.

Consider the scheme depicted in Figure 1 comprising two DGUs denoted with  $i$  and  $j$  and connected through a DC line with an impedance specified by parameters  $R_{ij} > 0$  and  $L_{ij} > 0$ . At each DGU level, a DC voltage source represents a generic renewable resource and a Buck converter is present in order to supply a local DC load connected to the PCC through a series  $LC$  filter. For instance, the DC load can be a combination of resistive electronic loads and negative resistance of constant power loads. Furthermore, we assume that loads are unknown and we treat them as current disturbances ( $I_L$ ) [4, 19].

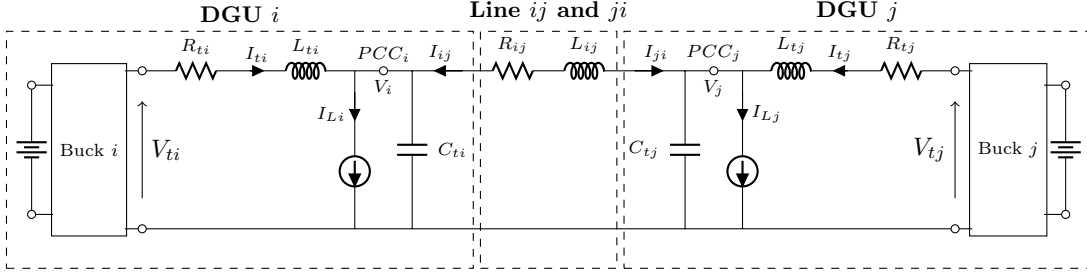


Figure 1: Electrical scheme of a DC ImG composed of two radially connected DGUs with unmod- elled loads.

Applying Kirchoff's voltage law and Kirchoff's current law to the electrical scheme of Figure 1, it is possible to write the following set of equations:

$$\text{DGU } i: \begin{cases} \frac{dV_i}{dt} = \frac{1}{C_{ti}}I_{ti} + \frac{1}{C_{ti}}I_{ij} - \frac{1}{C_{ti}}I_{Li} \\ \frac{dI_{ti}}{dt} = -\frac{R_{ti}}{L_{ti}}I_{ti} - \frac{1}{L_{ti}}V_i + \frac{1}{L_{ti}}V_{ti} \end{cases} \quad (1a)$$

$$(1b)$$

$$\text{Line } ij: \begin{cases} \frac{dI_{ij}}{dt} = \frac{1}{L_{ij}}V_j - \frac{R_{ij}}{L_{ij}}I_{ij} - \frac{1}{L_{ij}}V_i \end{cases} \quad (1c)$$

$$\text{Line } ji: \begin{cases} \frac{dI_{ji}}{dt} = \frac{1}{L_{ji}}V_i - \frac{R_{ji}}{L_{ji}}I_{ji} - \frac{1}{L_{ji}}V_j \end{cases} \quad (1d)$$

$$\text{DGU } j: \begin{cases} \frac{dV_j}{dt} = \frac{1}{C_{tj}}I_{tj} + \frac{1}{C_{tj}}I_{ji} - \frac{1}{C_{tj}}I_{Lj} \\ \frac{dI_{tj}}{dt} = -\frac{R_{tj}}{L_{tj}}I_{tj} - \frac{1}{L_{tj}}V_j + \frac{1}{L_{tj}}V_{tj} \end{cases} \quad (1e)$$

$$(1f)$$

As in [4], we notice that from (1c) and (1d) one gets two opposite line currents  $I_{ij}$  and  $I_{ji}$ . This is equivalent to have a reference current entering in each DGU. We exploit the following assumption to ensure that  $I_{ij}(t) = -I_{ji}(t)$ ,  $\forall t \geq 0$ .

**Assumption 1.** Initial states for the line currents fulfill  $I_{ij}(0) = -I_{ji}(0)$ . Furthermore, we set  $L_{ij} = L_{ji}$  and  $R_{ij} = R_{ji}$ .

**Remark 1.** According to the terminology in Section 3.4 of [20], the system in (1c), (1d) represents an expansion of the line model one obtains introducing only a single state variable. System (1) can also be viewed as a system of differential-algebraic equations, given by (1a)-(1c), (1e), (1f) and  $I_{ij}(t) = -I_{ji}(t)$ .

At this point, we notice that adopting the above notation for the lines, both DGU models have the same structure. In particular, by recalling that the load current  $I_{L*}$ ,  $* \in i, j$  is treated as a disturbance, (1) is the following linear system

$$\begin{aligned} \dot{x}(t) &= Ax(t) + Bu(t) + Md(t) \\ y(t) &= Cx(t) \end{aligned} \quad (2)$$

where  $x = [V_i, I_{ti}, I_{ij}, I_{ji}, V_j, I_{tj}]^T$  is the state,  $u = [V_{ti}, V_{tj}]^T$  the input,  $d = [I_{Li}, I_{Lj}]^T$  the disturbance and  $y = [V_i, V_j]^T$  the output of the system. All matrices in (2), which are obtained from (1), are given in Appendix A.1.

Next, we show how to describe each DGU as a dynamical system affected directly by state of the other DGU connected to it. An approximate model will be proposed so that there will be no need of using the line current in the DGU state equations.

## 2.1 QSL model

As in [16] and [21], we set  $\frac{dI_{ij}}{dt} = 0$  and  $\frac{dI_{ji}}{dt} = 0$ . Consequently, from (1c) and (1d), one gets the QSL model

$$\begin{aligned}\bar{I}_{ij} &= \frac{V_j}{R_{ij}} - \frac{V_i}{R_{ij}} \\ \bar{I}_{ji} &= \frac{V_i}{R_{ji}} - \frac{V_j}{R_{ji}}\end{aligned}\tag{3}$$

By replacing variables  $I_{ij}$  and  $I_{ji}$  in (1a) and (1e) with the right-hand side of (3), we obtain the following model of DGU  $i$

$$\text{DGU } i : \begin{cases} \frac{dV_i}{dt} = \frac{1}{C_{ti}}I_{ti} - \frac{1}{C_{ti}}I_{Li} + \frac{1}{C_{ti}}\bar{I}_{ij} \\ \frac{dI_{ti}}{dt} = -\frac{1}{L_{ti}}V_i - \frac{R_{ti}}{L_{ti}}I_{ti} + \frac{1}{L_{ti}}V_{ti} \end{cases}\tag{4}$$

Switching indexes  $i$  and  $j$  in (4) one obtains the model of DGU  $i$

$$\Sigma_{[i]}^{DGU} : \begin{cases} \dot{x}_{[i]}(t) = A_{ii}x_{[i]}(t) + B_i u_{[i]}(t) + M_i d_{[i]}(t) + \xi_{[i]}(t) \\ y_{[i]}(t) = C_i x_{[i]}(t) \\ z_{[i]}(t) = H_i y_{[i]}(t) \end{cases}\tag{5}$$

where  $x_{[i]} = [V_i, I_{ti}]^T$  is the state,  $u_{[i]} = V_{ti}$  the control input,  $d_{[i]} = I_{Li}$  the exogenous input and  $z_{[i]} = V_i$  the controlled variable of the system. Moreover,  $y_{[i]}(t)$  is the measurable output and we assume  $y_{[i]} = x_{[i]}$ , while  $\xi_{[i]}(t) = A_{ij}x_{[j]}$  represents the coupling with DGU  $j$ .

The matrices of  $\Sigma_{[i]}^{DGU}$  are obtained from (4) and they are provided in Appendix A.2. As regards the line, we obtain the subsystem

$$\Sigma_{[ij]}^{Line} : \{\dot{x}_{[l,ij]}(t) = A_{ll,ij}x_{[l,ij]}(t) + A_{li,ij}x_{[i]}(t) + A_{lj,ij}x_{[j]}(t)\}\tag{6}$$

with  $x_{[l,ij]} = I_{ij}$  as the state of the line. The matrices of (6) are derived from (1c) and reported in Appendix A.2. We have now all the ingredients to write the model of the overall microgrid depicted in Figure 1. In particular, from equations (5) and (6), we get

$$\begin{aligned}\begin{bmatrix} \dot{x}_{[i]} \\ \dot{x}_{[j]} \\ \dot{x}_{[l,ij]} \\ \dot{x}_{[l,ji]} \end{bmatrix} &= \begin{bmatrix} A_{ii} & A_{ij} & 0 & 0 \\ A_{ji} & A_{jj} & 0 & 0 \\ A_{li,ij} & A_{lj,ij} & A_{ll,ij} & 0 \\ A_{li,ji} & A_{lj,ji} & 0 & A_{ll,ji} \end{bmatrix} \begin{bmatrix} x_{[i]} \\ x_{[j]} \\ x_{[l,ij]} \\ x_{[l,ji]} \end{bmatrix} + \begin{bmatrix} B_i & 0 \\ 0 & B_j \\ 0 & 0 \\ 0 & 0 \end{bmatrix} \begin{bmatrix} u_{[i]} \\ u_{[j]} \end{bmatrix} + \begin{bmatrix} M_i & 0 \\ 0 & M_j \\ 0 & 0 \\ 0 & 0 \end{bmatrix} \begin{bmatrix} d_{[i]} \\ d_{[j]} \end{bmatrix} \\ \begin{bmatrix} y_{[i]} \\ y_{[j]} \end{bmatrix} &= \begin{bmatrix} C_1 & 0 & 0 & 0 \\ 0 & C_2 & 0 & 0 \end{bmatrix} \begin{bmatrix} x_{[i]} \\ x_{[j]} \\ x_{[l,ij]} \\ x_{[l,ji]} \end{bmatrix} \\ \begin{bmatrix} z_{[i]} \\ z_{[j]} \end{bmatrix} &= \begin{bmatrix} H_i & 0 \\ 0 & H_j \end{bmatrix} \begin{bmatrix} y_{[i]} \\ y_{[j]} \end{bmatrix}.\end{aligned}\tag{7}$$

**Remark 2.** Consider the structure of matrix  $A$

$$A = \left[ \begin{array}{cc|cc} A_{ii} & A_{ij} & 0 & 0 \\ A_{ji} & A_{jj} & 0 & 0 \\ \hline A_{li,ij} & A_{lj,ij} & A_{ll,ij} & 0 \\ A_{li,ji} & A_{lj,ji} & 0 & A_{ll,ji} \end{array} \right]$$

We notice that  $A$  is block-triangular, therefore its eigenvalues are given by the union of those of  $\begin{bmatrix} A_{ii} & A_{ij} \\ A_{ji} & A_{jj} \end{bmatrix}$ ,  $A_{ll,ij}$  and  $A_{ll,ji}$ . Moreover, we have  $A_{ll,ij} = A_{ll,ji}$ . By virtue of the positivity of the line parameters, line dynamics is asymptotically stable. As a consequence, stability of (7) depends on the stability of local DGUs connected through the QSL model (3). Hence, designing decentralized controllers  $u_{[*]} = k_{*}(y_{[*]})$ ,  $* \in \{i, j\}$ , such that the connection of the DGUs is asymptotically stable implies stability of the overall closed-loop model of the microgrid. We refer to the resulting system as QSL-ImG model.

## 2.2 QSL model of a microgrid composed of $N$ DGUs

In this section, a generalization of model (5) to ImGs composed of  $N$  DGUs is presented. Let  $\mathcal{D} = \{1, \dots, N\}$ . First, we call two DGUs neighbours if there is a transmission line connecting them. Then, we denote with  $\mathcal{N}_i \subset \mathcal{D}$  the subset of neighbours of DGU  $i$ . We highlight that the neighbouring relation is symmetric, consequently  $j \in \mathcal{N}_i$  implies  $i \in \mathcal{N}_j$ . In order to describe the dynamics of DGU  $i$ , we use model (5), with  $\xi_{[i]} = \sum_{j \in \mathcal{N}_i} A_{ij} x_{[j]}(t)$ . The new matrices of  $\Sigma_{[i]}^{DGU}$  are given in Appendix A.3 while the overall QSL-ImG model can be written as follows

$$\dot{\mathbf{x}}(t) = \mathbf{A}\mathbf{x}(t) + \mathbf{B}\mathbf{u}(t) + \mathbf{M}\mathbf{d}(t) \quad (8a)$$

$$\dot{x}_{[l,ij]}(t) = A_{ll,ij}x_{[l,ij]}(t) + A_{li,ij}x_{[i]}(t) + A_{lj,ij}x_{[j]}(t), \quad \forall i \in \mathcal{D}, \quad \forall j \in \mathcal{N}_i \quad (8b)$$

$$\begin{aligned} \mathbf{y}(t) &= \mathbf{C}\mathbf{x}(t) \\ \mathbf{z}(t) &= \mathbf{H}\mathbf{y}(t) \end{aligned} \quad (9)$$

where  $\mathbf{x} = (x_{[1]}, \dots, x_{[N]}) \in \mathbb{R}^{2N}$ ,  $\mathbf{u} = (u_{[1]}, \dots, u_{[N]}) \in \mathbb{R}^N$ ,  $\mathbf{d} = (d_{[1]}, \dots, d_{[N]}) \in \mathbb{R}^N$ ,  $\mathbf{y} = (y_{[1]}, \dots, y_{[N]}) \in \mathbb{R}^{2N}$ ,  $\mathbf{z} = (z_{[1]}, \dots, z_{[N]}) \in \mathbb{R}^N$ . Matrices  $\mathbf{A}$ ,  $A_{ll,ij}$ ,  $A_{li,ij}$ ,  $A_{lj,ij}$ ,  $\mathbf{B}$ ,  $\mathbf{M}$ ,  $\mathbf{C}$  and  $\mathbf{H}$  are reported in Appendix A.2 and A.3.

Note that neither  $\mathbf{y}$  nor  $\mathbf{z}$  depend upon states  $x_{[l,ij]}$ . Moreover, even  $x_{[l,ij]}$  does not influence  $\mathbf{x}$ . Hence, equations (8b) will be omitted in the sequel.

## 3 Plug-and-Play decentralized voltage control

### 3.1 Decentralized control scheme with integrators

Let  $\mathbf{z}_{\text{ref}}(t)$  denote the constant desired reference trajectory for the output  $\mathbf{z}(t)$ . In order to track asymptotically  $\mathbf{z}_{\text{ref}}(t)$  when  $\mathbf{d}(t)$  is constant, we consider the augmented ImG model with integrators [22]. A necessary condition for having that the steady-state error  $\mathbf{e}(t) = \mathbf{z}_{\text{ref}}(t) - \mathbf{z}(t)$  tends to zero as  $t \rightarrow \infty$ , is that for arbitrary constant signals  $\mathbf{d}(t) = \bar{\mathbf{d}}$  and  $\mathbf{z}_{\text{ref}}(t) = \bar{\mathbf{z}}_{\text{ref}}$ , there are equilibrium states and inputs  $\bar{\mathbf{x}}$  and  $\bar{\mathbf{u}}$  verifying

$$\begin{aligned} \mathbf{0} &= \mathbf{A}\bar{\mathbf{x}} + \mathbf{B}\bar{\mathbf{u}} + \mathbf{M}\bar{\mathbf{d}} \\ \bar{\mathbf{z}}_{\text{ref}} &= \mathbf{H}\mathbf{C}\bar{\mathbf{x}} \end{aligned} \quad (10)$$

$$\Gamma \begin{bmatrix} \bar{\mathbf{x}} \\ \bar{\mathbf{u}} \end{bmatrix} = \begin{bmatrix} \mathbf{0} & -\mathbf{M} \\ \mathbf{I} & \mathbf{0} \end{bmatrix} \begin{bmatrix} \bar{\mathbf{z}}_{\text{ref}} \\ \bar{\mathbf{d}} \end{bmatrix}, \quad \Gamma = \begin{bmatrix} \mathbf{A} & \mathbf{B} \\ \mathbf{H}\mathbf{C} & \mathbf{0} \end{bmatrix} \in \mathbb{R}^{3N \times 3N} \quad (11)$$

**Proposition 1.** Given  $\bar{\mathbf{z}}_{\text{ref}}$  and  $\bar{\mathbf{d}}$ , vectors  $\bar{\mathbf{x}}$  and  $\bar{\mathbf{u}}$  satisfying (11) always exist.

*Proof.* From [22], we know that exists  $\bar{\mathbf{x}}, \bar{\mathbf{u}}$  verifying (11) if and only if the following two conditions are fulfilled:

- (i) The number of controlled variables is not greater than the number of control inputs.
- (ii) The system under control has no invariant zeros (i.e.  $\text{rank}(\Gamma) = 3N$ ).

Condition (i) is fulfilled since from (5) one has that  $u_{[i]}$  and  $z_{[i]}$  have the same size,  $\forall i \in \mathcal{D}$ . In order to prove Condition (ii), we exploit the definition of matrices  $\mathbf{A}$ ,  $\mathbf{B}$ ,  $\mathbf{C}$  and  $\mathbf{H}$  and the fact that electrical parameters are positive.  $\square$

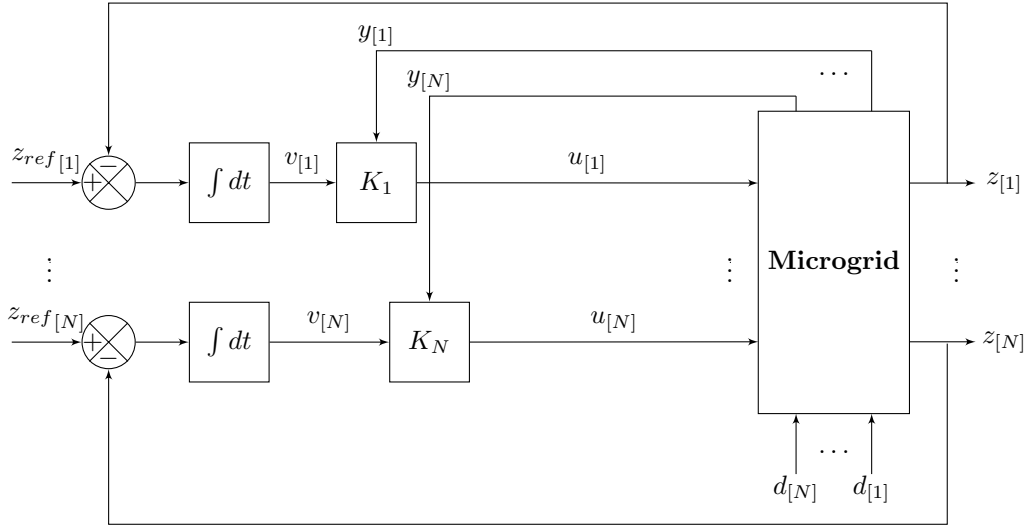


Figure 2: Control scheme with integrators for the overall augmented model.

The dynamics of the integrators is (see Figure 2)

$$\begin{aligned} \dot{v}_{[i]}(t) &= e_{[i]}(t) = z_{ref[i]}(t) - z_{[i]}(t) \\ &= z_{ref[i]}(t) - H_i C_i x_{[i]}(t), \end{aligned} \quad (12)$$

and hence, the DGU model augmented with integrators is

$$\hat{\Sigma}_{[i]}^{DGU} : \begin{cases} \dot{\hat{x}}_{[i]}(t) = \hat{A}_{ii} \hat{x}_{[i]}(t) + \hat{B}_i u_{[i]}(t) + \hat{M}_i \hat{d}_{[i]}(t) + \hat{\xi}_{[i]}(t) \\ \hat{y}_{[i]}(t) = \hat{C}_i \hat{x}_{[i]}(t) \\ z_{[i]}(t) = \hat{H}_i \hat{y}_{[i]}(t) \end{cases} \quad (13)$$

where  $\hat{x}_{[i]} = [x_{[i]}^T, v_{[i]}]^T \in \mathbb{R}^3$  is the state,  $\hat{y}_{[i]} = \hat{x}_{[i]} \in \mathbb{R}^3$  is the measurable output,  $\hat{d}_{[i]} = [d_{[i]}, z_{ref[i]}]^T \in \mathbb{R}^2$  collects the exogenous signals (both current of the load and reference signals) and  $\hat{\xi}_{[i]}(t) = \sum_{j \in \mathcal{N}_i} \hat{A}_{ij} \hat{x}_{[j]}(t)$ . Matrices in (13) are defined as follows

$$\hat{A}_{ii} = \begin{bmatrix} A_{ii} & 0 \\ -H_i C_i & 0 \end{bmatrix} \hat{A}_{ij} = \begin{bmatrix} A_{ij} & 0 \\ 0 & 0 \end{bmatrix} \hat{B}_i = \begin{bmatrix} B_i \\ 0 \end{bmatrix} \hat{C}_i = \begin{bmatrix} C_i & 0 \\ 0 & I \end{bmatrix} \hat{M}_i = \begin{bmatrix} M_i & 0 \\ 0 & 1 \end{bmatrix} \hat{H}_i = [H_i \quad 0]. \quad (14)$$

Through the following proposition we make sure that the pair  $(\hat{A}_{ii}, \hat{B}_i)$  is controllable, thus system (13) can be stabilized.

**Proposition 2.** *The pair  $(\hat{A}_{ii}, \hat{B}_i)$  is controllable.*

*Proof.* Using the definition of controllability matrix, we get

$$\begin{aligned}\hat{M}_i^C &= [\hat{B}_i \quad \hat{A}_{ii}\hat{B}_i \quad \hat{A}_{ii}^2\hat{B}_i] \\ &= \underbrace{\begin{bmatrix} A_{ii} & B_i \\ -H_i C_i & 0 \end{bmatrix}}_{\hat{M}_{i,1}^C} \underbrace{\begin{bmatrix} 0 & B_i & A_{ii}B_i & A_{ii}^2 B_i \\ I & 0 & 0 & 0 \end{bmatrix}}_{\hat{M}_{i,2}^C}.\end{aligned}\quad (15)$$

Matrices  $\hat{M}_{i,1}^C$  and  $\hat{M}_{i,2}^C$  have always full rank, since all electrical parameters are positive, hence  $\text{rank}(\hat{M}_i^C) = 3$ . Therefore the pair  $(\hat{A}_{ii}, \hat{B}_i)$  is controllable.  $\square$

The overall augmented system is obtained from (13) as

$$\begin{cases} \dot{\hat{\mathbf{x}}}(t) = \hat{\mathbf{A}}\hat{\mathbf{x}}(t) + \hat{\mathbf{B}}\mathbf{u}(t) + \hat{\mathbf{M}}\hat{\mathbf{d}}(t) \\ \hat{\mathbf{y}}(t) = \hat{\mathbf{C}}\hat{\mathbf{x}}(t) \\ \mathbf{z}(t) = \hat{\mathbf{H}}\hat{\mathbf{y}}(t) \end{cases}\quad (16)$$

where  $\hat{\mathbf{x}}$ ,  $\hat{\mathbf{y}}$  and  $\hat{\mathbf{d}}$  collect variables  $\hat{x}_{[i]}$ ,  $\hat{y}_{[i]}$  and  $\hat{d}_{[i]}$  respectively, and matrices  $\hat{\mathbf{A}}$ ,  $\hat{\mathbf{B}}$ ,  $\hat{\mathbf{C}}$ ,  $\hat{\mathbf{M}}$  and  $\hat{\mathbf{H}}$  are obtained from systems (13).

### 3.2 Decentralized PnP control

This section presents the adopted control approach that allows us to design local controlles while guaranteeing asymptotic stability for the augmented system (16). Local controllers are synthesized in a decentralized fashion permitting PnP operations. Let us equip each DGU  $\hat{\Sigma}_{[i]}^{DGU}$  with the following state-feedback controller

$$\mathcal{C}_{[i]} : \quad u_{[i]}(t) = K_i \hat{y}_{[i]}(t) = K_i \hat{x}_{[i]}(t) \quad (17)$$

where  $K_i \in \mathbb{R}^{1 \times 3}$  and controllers  $\mathcal{C}_{[i]}$ ,  $i \in \mathcal{D}$  are decentralized since the computation of  $u_{[i]}(t)$  requires the state of  $\hat{\Sigma}_{[i]}^{DGU}$  only. Let nominal subsystems be given by  $\hat{\Sigma}_{[i]}^{DGU}$  without coupling terms  $\hat{\xi}_{[i]}(t)$ . We aim to design local controllers  $\mathcal{C}_{[i]}$  such that the nominal closed-loop subsystem

$$\begin{cases} \dot{\hat{x}}_{[i]}(t) = (\hat{A}_{ii} + \hat{B}_i K_i) \hat{x}_{[i]}(t) + \hat{M}_i \hat{d}_{[i]}(t) \\ \hat{y}_{[i]}(t) = \hat{C}_i \hat{x}_{[i]}(t) \\ z_{[i]}(t) = \hat{H}_i \hat{y}_{[i]}(t) \end{cases}\quad (18)$$

is asymptotically stable. From Lyapunov theory, we know that if there exists a symmetric matrix  $P_i \in \mathbb{R}^{3 \times 3}$ ,  $P_i > 0$  such that

$$(\hat{A}_{ii} + \hat{B}_i K_i)^T P_i + P_i (\hat{A}_{ii} + \hat{B}_i K_i) < 0, \quad (19)$$

then the nominal closed-loop subsystem equipped with controller  $\mathcal{C}_{[i]}$  is asymptotically stable. Similarly, the closed-loop QSL-ImG be given by (16) and (17)

$$\begin{cases} \dot{\hat{\mathbf{x}}}(t) = (\hat{\mathbf{A}} + \hat{\mathbf{B}}\mathbf{K})\hat{\mathbf{x}}(t) + \hat{\mathbf{M}}\hat{\mathbf{d}}(t) \\ \hat{\mathbf{y}}(t) = \hat{\mathbf{C}}\hat{\mathbf{x}}(t) \\ \mathbf{z}(t) = \hat{\mathbf{H}}\hat{\mathbf{y}}(t) \end{cases}\quad (20)$$

is asymptotically stable if matrix  $\mathbf{P} = \text{diag}(P_1, \dots, P_N)$  satisfies

$$(\hat{\mathbf{A}} + \hat{\mathbf{B}}\mathbf{K})^T \mathbf{P} + \mathbf{P}(\hat{\mathbf{A}} + \hat{\mathbf{B}}\mathbf{K}) < 0 \quad (21)$$

where  $\hat{\mathbf{A}}$ ,  $\hat{\mathbf{B}}$  and  $\mathbf{K}$  collect matrices  $\hat{A}_{ij}$ ,  $\hat{B}_i$  and  $K_i$ , for all  $i, j \in \mathcal{D}$ . We want to emphasize that, in general, (19) does not imply (21), since one can show that decentralized design of local controllers

can fail to guarantee voltage stability of the whole ImG, if coupling among DGUs is neglected (see Appendix B in [5] for an example in the case of AC ImGs). In order to derive conditions such that (19) guarantees (21), we first define  $\hat{\mathbf{A}}_{\mathbf{D}} = \text{diag}(\hat{A}_{ii}, \dots, \hat{A}_{NN})$  and  $\hat{\mathbf{A}}_{\mathbf{C}} = \hat{\mathbf{A}} - \hat{\mathbf{A}}_{\mathbf{D}}$ . Then, we exploit the following assumptions to ensure asymptotic stability of the closed-loop QSL-ImG.

**Assumption 2.** (i) Decentralized controllers  $\mathcal{C}_{[i]}$ ,  $i \in \mathcal{D}$  are designed such that (19) holds with

$$P_i = \left( \begin{array}{c|cc} \eta_i & 0 & 0 \\ \hline 0 & \bullet & \bullet \\ 0 & \bullet & \bullet \end{array} \right) \quad (22)$$

where  $\bullet$  denotes an arbitrary entry and  $\eta_i > 0$  is a local parameter.

(ii) It holds  $\frac{\eta_i}{R_{ij}C_{ti}} \approx 0$ ,  $\forall i \in \mathcal{D}$ ,  $\forall j \in \mathcal{N}_i$ .

As regards Assumption 2-(i), we will show later that checking the existence of  $P_i$  as in (22) and  $K_i$  fulfilling (19) leads to solving a convex optimization problem. On the other hand, there exist different ways to fulfill Assumption 2-(ii). In fact, when an upper bound to all ratios  $\frac{1}{R_{ij}C_{ti}}$  (which depend upon line parameters only) is known, one can simply set the control design parameter  $\eta_i$  sufficiently small. However, if networks are spread over a small area, the impedances are small and predominantly resistive. Therefore, one has  $\frac{1}{R_{ij}C_{ti}} \approx 0$  by construction and bigger values of  $\eta_i$  can be used for synthesizing local controllers.

**Proposition 3.** Let Assumption 2 holds. Then, the overall closed-loop QSL-ImG is asymptotically stable.

*Proof.* We have to show that (21) holds, which is equivalent to prove that

$$\underbrace{(\hat{\mathbf{A}}_{\mathbf{D}} + \hat{\mathbf{B}}\mathbf{K})^T \mathbf{P} + \mathbf{P}(\hat{\mathbf{A}}_{\mathbf{D}} + \hat{\mathbf{B}}\mathbf{K})}_{(a)} + \underbrace{\hat{\mathbf{A}}_{\mathbf{C}}^T \mathbf{P} + \mathbf{P}\hat{\mathbf{A}}_{\mathbf{C}}}_{(b)} < 0. \quad (23)$$

First, we highlight that term (a) is a block diagonal matrix that collects on the diagonal all left hand sides of (19). It follows that term (a) is a negative definite matrix. Next, we show that term (b) is zero. In particular, each block  $(i, j)$  of term (b) can be written as

$$\begin{cases} P_i \hat{A}_{ij} + \hat{A}_{ji}^T P_j & \text{if } j \in \mathcal{N}_i \\ 0 & \text{otherwise} \end{cases}$$

Using Assumption 2-(ii), we obtain

$$P_i \hat{A}_{ij} = \begin{pmatrix} \frac{\eta_i}{R_{ij}C_{ti}} & 0 & 0 \\ 0 & 0 & 0 \\ 0 & 0 & 0 \end{pmatrix} \approx \begin{pmatrix} 0 & 0 & 0 \\ 0 & 0 & 0 \\ 0 & 0 & 0 \end{pmatrix} \quad (24)$$

and

$$\hat{A}_{ji}^T P_j = \begin{pmatrix} \frac{\eta_j}{R_{ji}C_{tj}} & 0 & 0 \\ 0 & 0 & 0 \\ 0 & 0 & 0 \end{pmatrix} \approx \begin{pmatrix} 0 & 0 & 0 \\ 0 & 0 & 0 \\ 0 & 0 & 0 \end{pmatrix}, \quad (25)$$

which proves that inequality (23) holds.  $\square$

At this point, in order to complete the design of the local controller  $\mathcal{C}_{[i]}$ , we have to solve the following problem.



**Problem 1.** Compute a matrix  $K_i$  such that the nominal closed-loop subsystem is asymptotically stable and Assumption 2-(i) is verified, i.e. (19) holds for a matrix  $P_i$  structured as in (22).

Consider the following optimization problem

$$\begin{aligned} \mathcal{O} : \min_{Y_i, G_i, \gamma_i, \beta_i, \delta_i} \quad & \alpha_{i1}\gamma_i + \alpha_{i2}\beta_i + \alpha_{i3}\delta_i \\ Y_i = \begin{bmatrix} \eta_i^{-1} & 0 & 0 \\ 0 & \ddots & \\ 0 & & \ddots \end{bmatrix} & > 0 \end{aligned} \quad (26a)$$

$$\begin{bmatrix} Y_i \hat{A}_{ii}^T + G_i^T \hat{B}_i^T + \hat{A}_{ii} Y_i + \hat{B}_i G_i & Y_i \\ Y_i & -\gamma_i I \end{bmatrix} \leq 0 \quad (26b)$$

$$\begin{bmatrix} -\beta_i I & G_i^T \\ G_i & -I \end{bmatrix} < 0 \quad (26c)$$

$$\begin{bmatrix} Y_i & I \\ I & \delta_i I \end{bmatrix} > 0 \quad (26d)$$

$$\gamma_i > 0, \quad \beta_i > 0, \quad \delta_i > 0 \quad (26e)$$

where  $\alpha_{i1}$ ,  $\alpha_{i2}$  and  $\alpha_{i3}$  represent positive weights and  $\bullet$  are arbitrary entries. Since all constraints in (26) are Linear Matrix Inequalities (LMI), the optimization problem is convex and can be solved with efficient (i.e. polynomial-time) LMI solvers [23].

**Lemma 1.** Problem  $\mathcal{O}$  is feasible if and only if Problem 1 has a solution. Moreover,  $K_i$  and  $P_i$  in (19) are given by  $K_i = G_i Y_i^{-1}$ ,  $P_i = Y_i^{-1}$  and  $\|K_i\|_2 < \sqrt{\beta_i} \delta_i$ .

*Proof.* Inequality (19) is equivalent to the existence of  $\gamma_i > 0$  such that

$$(\hat{A}_{ii} + \hat{B}_i K_i)^T P_i + P_i (\hat{A}_{ii} + \hat{B}_i K_i) + \gamma_i^{-1} I \leq 0 \quad (27)$$

where  $P_i$  is defined in (22). By applying the Schur lemma on (27), we get the following inequality

$$\begin{bmatrix} (\hat{A}_{ii} + \hat{B}_i K_i)^T P_i + P_i (\hat{A}_{ii} + \hat{B}_i K_i) & I \\ I & -\gamma_i I \end{bmatrix} \leq 0 \quad (28)$$

which is nonlinear in  $P_i$  and  $K_i$ . In order to get rid of the nonlinear terms, we perform the following parametrization trick [23]

$$\begin{aligned} Y_i &= P_i^{-1} \\ G_i &= K_i Y_i. \end{aligned} \quad (29)$$

Notice that the structure of  $Y_i$  is the same as the structure of  $P_i$ . By pre- and post-multiplying (28) with  $\begin{bmatrix} Y_i & 0 \\ 0 & I \end{bmatrix}$  and exploiting (29) we obtain

$$\begin{bmatrix} Y_i \hat{A}_{ii}^T + G_i^T \hat{B}_i^T + \hat{A}_{ii} Y_i + \hat{B}_i G_i & Y_i \\ Y_i & -\gamma_i I \end{bmatrix} \leq 0 \quad (30)$$

Constraint (26a) ensures that matrix  $P_i$  has the structure required by Assumption 2-(i). At the same time, constraint (26b) guarantees stability of the closed-loop subsystem. Further constraints appear in Problem  $\mathcal{O}$  with the aim of bounding  $\|K_i\|_2$ . In particular, we add  $\|G_i\|_2 < \sqrt{\beta_i}$  and  $\|Y_i^{-1}\|_2 < \delta_i$  (which via Schur complement, correspond to constraints (26c) and (26d)) to prevent  $\|K_i\|_2$  from becoming too large. These bounds imply  $\|K_i\|_2 < \sqrt{\beta_i} \delta_i$  and then affect the magnitude of control variables.  $\square$

Next, we discuss the key feature of the proposed decentralized control approach. We first notice that constraints in (26) depend upon local fixed matrices  $(\hat{A}_{ii}, \hat{B}_i)$  and local design parameters  $(\alpha_{i1}, \alpha_{i2}, \alpha_{i3}, \beta_i, \delta_i)$ . It follows that the computation of controller  $\mathcal{C}_{[i]}$  is completely independent from the computation of controllers  $\mathcal{C}_{[j]}$  when  $j \neq i$  since, provided that problem  $\mathcal{P}_i$  is feasible, controller  $\mathcal{C}_{[i]}$  can be directly obtained through  $K_i = G_i Y_i^{-1}$ . In addition, it is clear that constraints (26c) and (26d) affect only the magnitude of control variables as stated in Lemma 1. Finally, since all assumptions in Proposition 3 are verified, the overall closed-loop QSL-ImG is asymptotically stable.

### 3.3 Enhancements of local controllers for improving performances

In the previous section we have shown how to design decentralized controllers  $\mathcal{C}_{[i]}$  guaranteeing asymptotic stability for the overall closed-loop system (20). In order to improve transient performances of controllers  $\mathcal{C}_{[i]}$ , we enhance them with feed-forward terms for

- (i) pre-filtering reference signals;
- (ii) compensating measurable disturbances.

#### 3.3.1 Pre-filtering of the reference signal

Pre-filtering is well known technique used to widen the bandwidth so as to speed up the response of the system. Consider the transfer function  $F_{[i]}(s)$ , from  $z_{ref[i]}(t)$  to the controlled variable  $z_{[i]}(t)$

$$F_{[i]}(s) = (\hat{H}_i \hat{C}_i)(sI - (\hat{A}_{ii} + \hat{B}_i K_i))^{-1} \begin{bmatrix} 0 \\ 1 \end{bmatrix} \quad (31)$$

of each nominal closed-loop subsystem (18). By virtue of a feedforward compensator  $\tilde{C}_{[i]}(s)$ , it is possible to filter the reference signal  $z_{ref[i]}(t)$  (see Figure 3). Consequently, the new transfer

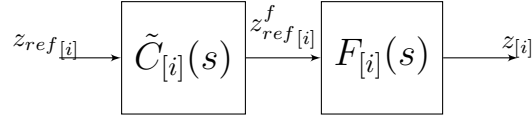


Figure 3: Block diagram of closed-loop DGU  $i$  with prefilter.

function from  $z_{ref[i]}(t)$  to  $z_{[i]}(t)$  becomes

$$\tilde{F}_{[i]}(s) = \tilde{C}_{[i]}(s)F_{[i]}(s) \quad (32)$$

Now, taking a desired transfer function  $\tilde{F}_{[i]}(s)$  for each subsystem, we can compute, from (32), the pre-filter  $\tilde{C}_{[i]}(s)$  as

$$\tilde{C}_{[i]}(s) = \tilde{F}_{[i]}(s)F_{[i]}(s)^{-1} \quad (33)$$

under the following conditions [22]:

- $F_{[i]}(s)$  must not have Right-Half-Plane (RHP) zeros that would become RHP poles of  $\tilde{C}_{[i]}(s)$ , making it unstable;
- $F_{[i]}(s)$  must not contain a time delay, otherwise  $\tilde{C}_{[i]}(s)$  would have a predictive action
- $\tilde{C}_{[i]}(s)$  must be realizable, i.e. it must have more poles than zeros.

Hence, if these conditions are fulfilled, the filter  $\tilde{C}_{[i]}(s)$  given by (33) is realizable and asymptotically stable (this condition is essential since  $\tilde{C}_{[i]}(s)$  works in open-loop). Furthermore, since  $\hat{F}_{[i]}(s)$  is asymptotically stable (controllers  $\mathcal{C}_{[i]}$  are, in fact, designed solving the problem  $\mathcal{P}_i$ ), the closed-loop system including filters  $\tilde{C}_{[i]}(s)$  is asymptotically stable as well. He highlight that, if some of the previous conditions are not valid, expression (33) cannot be used. Still, the compensator  $\tilde{C}_{[i]}(s)$  can be designed for a given bandwidth, as shown in [22].

### 3.3.2 Compensation of measurable disturbances

The second enhancement one can introduce regards the compensation of measurable disturbances. We remind that, since we assumed that load dynamics is not known, we have modeled the load currents for each subsystem of the microgrid as a measurable disturbance  $d_{[i]}(t)$ . Let us define new local controllers  $\tilde{\mathcal{C}}_{[i]}$  as

$$\tilde{\mathcal{C}}_{[i]} : \quad u_{[i]} = K_i \hat{x}_{[i]}(t) + \tilde{u}_{[i]}(t) \quad (34)$$

Note that  $\tilde{\mathcal{C}}_{[i]}$  are obtained by adding term  $\tilde{u}_{[i]}(t)$  to the controllers  $\mathcal{C}_{[i]}$  in (17). Hence, (18) can be rewritten as follows

$$\tilde{\Sigma}_{[i]}^{DGU} : \begin{cases} \dot{\hat{x}}_{[i]}(t) = (\hat{A}_{ii} + \hat{B}_i K_i) \hat{x}_{[i]}(t) + \hat{M}_i \hat{d}_{[i]}(t) + \hat{B}_i \tilde{u}_{[i]}(t) \\ \hat{y}_{[i]}(t) = \hat{C}_i \hat{x}_{[i]}(t) \\ z_{[i]}(t) = \hat{H}_i \hat{y}_{[i]}(t) \end{cases} \quad (35)$$

We now use the new input  $\tilde{u}_{[i]}(t)$  to compensate the measurable disturbance  $d_{[i]}(t)$  (recall that  $\hat{d}_{[i]} = [d_{[i]}^T \ z_{ref[i]}^T]^T$ ). From (35), the transfer function from the disturbance  $d_{[i]}(t)$  to the controlled variable  $z_{[i]}(t)$  is

$$G_i^d(s) = (\hat{H}_i \hat{C}_i)(sI - (\hat{A}_{ii} + \hat{B}_i K_i))^{-1} \begin{bmatrix} \hat{M}_i \\ 0 \end{bmatrix}. \quad (36)$$

Moreover, the transfer function from the new input  $\tilde{u}_{[i]}(t)$  to the controlled variable  $z_{[i]}(t)$  is

$$G_i(s) = (\hat{H}_i \hat{C}_i)(sI - (\hat{A}_{ii} + \hat{B}_i K_i))^{-1} \hat{B}_i. \quad (37)$$

If we combine (36) and (37), we obtain

$$z_{[i]}(s) = G_i(s) \tilde{u}_{[i]}(s) + G_i^d(s) d_{[i]}(s). \quad (38)$$

In order to zero the effect of the disturbance on the controlled variable, we set

$$\tilde{u}_{[i]}(s) = N_i(s) d_{[i]}(s) \quad (39)$$

where

$$N_{[i]}(s) = -G_i(s)^{-1} G_i^d(s) \quad (40)$$

is the transfer function of the compensator. Note that  $N_{[i]}(s)$  is well defined under the following conditions [22]:

- $G_{[i]}(s)$  must not have RHP zeros that would become RHP poles of  $N_{[i]}(s)$ ;
- $G_{[i]}(s)$  must not contain a time delay, otherwise  $N_{[i]}(s)$  would have a predictive action
- $N_{[i]}(s)$  must be realizable, i.e. it must have more poles than zeros.

In this way, we can ensure that the compensator  $N_{[i]}(s)$  is asymptotically stable, hence preserving asymptotic stability of the system. When some of the previous conditions do not hold, formula (40) cannot be used and perfect compensation cannot be achieved. Still, the compensator  $N_{[i]}(s)$  can be designed to reject disturbances within a given bandwidth, as shown in [22]. The overall control scheme with the addition of the compensators is shown in Figure 4.

## 3.4 Algorithm for the design of local controllers

Algorithm 1 collects the steps of the overall design procedure.

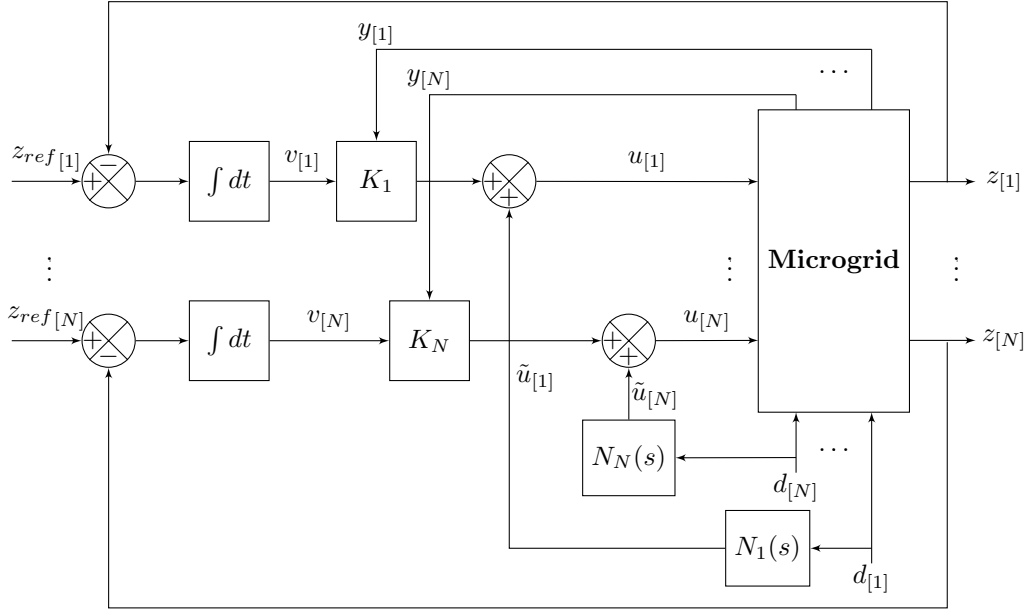


Figure 4: Overall microgrid control scheme with compensation of measurable disturbances  $d_{[i]}(s)$ .

---

**Algorithm 1** Design of controller  $\mathcal{C}_{[i]}$  and compensators  $\tilde{C}_{[i]}$  and  $N_{[i]}$  for subsystem  $\hat{\Sigma}_{[i]}^{DGU}$

---

**Input:** DGU  $\hat{\Sigma}_{[i]}^{DGU}$  as in (13)

**Output:** Controller  $\mathcal{C}_{[i]}$  and, optionally, pre-filter  $\tilde{C}_{[i]}$  and compensator  $N_{[i]}$

---

(A) Find  $K_i$  solving the LMI problem (26). If it is not feasible **stop** (the controller  $\mathcal{C}_{[i]}$  cannot be designed).

**Optional steps**

(B) Design the asymptotically stable local pre-filter  $\tilde{C}_{[i]}$  and compensator  $N_{[i]}$  as in (40).

---

### 3.5 PnP operations

In the following section, the operations for updating the controllers when DGUs are added to or removed from an ImG are presented. We remind that all these operations are performed with the aim of preserving stability of the new closed-loop system. Consider, as a starting point, a microgrid composed of subsystems  $\hat{\Sigma}_{[i]}^{DGU}, i \in \mathcal{D}$  equipped with local controllers  $\mathcal{C}_{[i]}$  and compensators  $\tilde{C}_{[i]}$  and  $N_{[i]}, i \in \mathcal{D}$  produced by Algorithm 1.

**Remark 3.** In order to avoid jumps in the control variable when local regulator are switched, we embed each local regulator into a bumpless control scheme [18] shown in Appendix B.

**Plugging-in operation** Assume that the plug-in of a new DGU  $\hat{\Sigma}_{[N+1]}^{DGU}$  described by matrices,  $\hat{A}_{N+1, N+1}, \hat{B}_{N+1}, \hat{C}_{N+1}, \hat{M}_{N+1}, \hat{H}_{N+1}$  and  $\{\hat{A}_{N+1, j}\}_{j \in \mathcal{N}_{N+1}}$  needs to be performed. Let  $\mathcal{N}_{N+1}$  be the set of DGUs that are directly coupled to  $\hat{\Sigma}_{[N+1]}^{DGU}$  through transmission lines and let  $\{\hat{A}_{N+1, j}\}_{j \in \mathcal{N}_{N+1}}$  be the matrices containing the corresponding coupling terms. According to our method, the design of controller  $\mathcal{C}_{[N+1]}$  and compensators  $\tilde{C}_{[N+1]}$  and  $N_{[N+1]}$  requires Algorithm 1 to be executed. Since DGUs  $\hat{\Sigma}_{[j]}^{DGU}, j \in \mathcal{N}_{N+1}$ , have the new neighbour  $\hat{\Sigma}_{[N+1]}^{DGU}$ , we need to re-design controllers  $\mathcal{C}_{[j]}$  and compensators  $\tilde{C}_{[j]}$  and  $N_{[j]}, \forall j \in \mathcal{N}_{N+1}$  because matrices  $\hat{A}_{jj}, j \in \mathcal{N}_{N+1}$  change.

Only if Algorithm 1 does not stop in Step A when computing controllers  $\mathcal{C}_{[k]}$  for all  $k \in \mathcal{N}_{N+1} \cup \{N+1\}$ , we have that the plug-in of  $\hat{\Sigma}_{[N+1]}^{DGU}$  is allowed. Moreover, we stress that the redesign is not propagated further in the network and therefore the asymptotic stability of the new overall closed-loop QSL-ImG model is preserved even without changing controllers  $\mathcal{C}_{[i]}$ ,  $\tilde{C}_{[i]}$  and  $N_{[i]}$ ,  $i \notin \{N+1\} \cup \mathcal{N}_{N+1}$ .

Prior to real-time plugging-in operation (*hot plugging-in*), it is recommended to keep set points constant for a sufficient amount of time so as to guarantee control variable in the bumpless control scheme (see Remark 3) is in steady state. This ensures smooth behaviours of the electrical variables.

**Unplugging operation** Let us now examine the unplugging of DGU  $\hat{\Sigma}_{[k]}^{DGU}$ ,  $k \in \mathcal{D}$ . The disconnection of  $\hat{\Sigma}_{[k]}^{DGU}$  from the network leads to a change in matrix  $\hat{A}_{jj}$  of each  $\hat{\Sigma}_{[j]}^{DGU}$ ,  $j \in \mathcal{N}_k$ . Consequently, for each  $j \in \mathcal{N}_k$ , we have to redesign controllers  $\mathcal{C}_{[j]}$  and compensators  $\tilde{C}_{[j]}$  and  $N_{[j]}$ . As for the plug-in operation, we run Algorithm 1. If all operations can be successfully terminated, then the unplugging of  $\hat{\Sigma}_{[k]}^{DGU}$  is allowed and stability is preserved without redesigning the local controllers  $\mathcal{C}_{[j]}$ ,  $j \notin \mathcal{N}_k$ .

When an unplugging operation is scheduled in advance, it is advisable to follow an *hot unplugging* protocol similar to the one introduced for the plugging-in operation.

## 4 Simulation results

In this section, we study performance brought about by PnP controllers described in Section 3. As a starting point, we consider the ImG depicted in Figure 1 with only two DGUs (Scenario 1) and we evaluate performance in terms of tracking step references as well as hot plugging-in of the two DGUs and robustness to unknown load dynamic. Then, we extend the analysis to an ImG with 6 DGUs (Scenario 2) and we show that stability of the whole microgrid is guaranteed.

Simulations have been performed in PSCAD, a simulation environment for electric systems which allows to implement the microgrid model with realistic electric components.

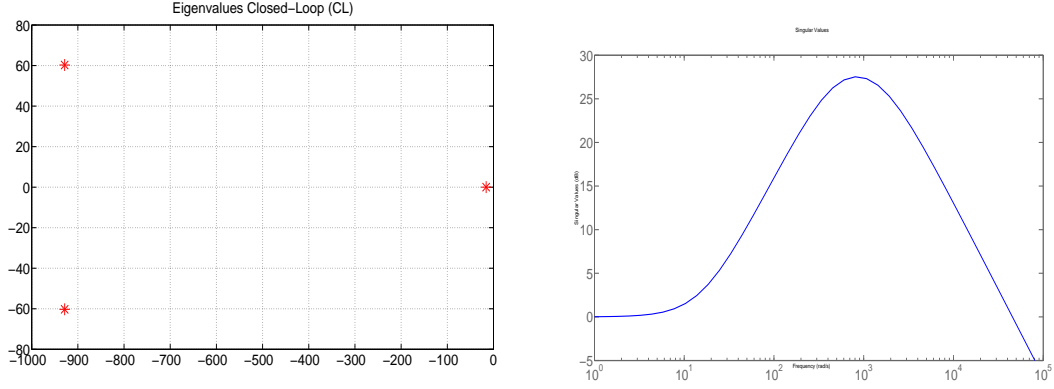
For both scenarios, we run a simulation from time 0 s up to time 10 s. Each simulation has been split into subparts that are discussed next.

### 4.1 Scenario 1

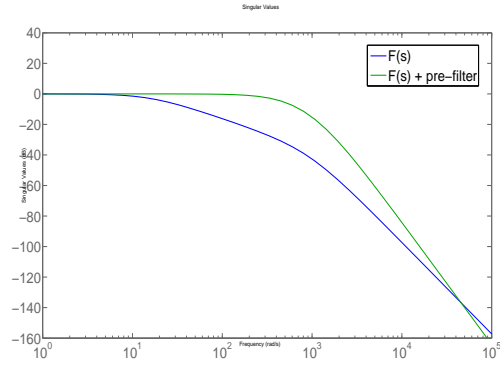
In this Scenario, we consider the ImG shown in Figure 1 composed of two DC DGUs connected through high resistive-inductive lines supporting 10  $\Omega$  and 6  $\Omega$  loads, respectively. For the sake of simplicity, we set  $i = 1$  and  $j = 2$ . The output voltage reference  $v_{MG}^*$  has been selected at 48 V and it is equal for both DGUs. Parameters values for all DGUs are given in Table 1 in Appendix C. Notice that that they are comparable to those used in [17] and [7].

#### 4.1.1 Voltage reference tracking at the startup

We assume that at the beginning of the simulation ( $t = 0$  s), subsystems  $\hat{\Sigma}_{[1]}^{DGU}$  and  $\hat{\Sigma}_{[2]}^{DGU}$  are not interconnected. Therefore, stabilizing controllers  $\mathcal{C}_i$ ,  $i = 1, 2$  are designed neglecting coupling among DGUs. Moreover, in order to widen the bandwidth of each closed-loop subsystem, we use local pre-filters  $\tilde{C}_{[i]}$ ,  $i = 1, 2$  of reference signals. The desired closed-loop transfer functions  $\tilde{F}_i(s)$ ,  $i = 1, 2$  have been chosen as low-pass filters with DC gain equal to 0 dB and bandwidth equal to 100 Hz. The eigenvalues of the two decoupled closed-loop QSL subsystems are shown in Figure 5a. Moreover, by running Step B of Algorithm 1 we obtain two asymptotically stable local pre-filters  $\tilde{C}_i$ ,  $i = 1, 2$  whose Bode magnitude plots are depicted in Figure 5b. Notice that through the addition of the pre-filters, the frequency response of the two closed-loop transfer functions  $F_i(s)$ ,  $i = 1, 2$  coincide with the frequency response of the desired transfer functions  $\tilde{F}_i(s)$ ,  $i = 1, 2$  (see the green line in Figure 5c). Figures 6a and 6b show the voltages at  $PCC_1$  and  $PCC_2$ . Note that the controllers ensure an excellent tracking of the reference signals at the startup in a very short time.

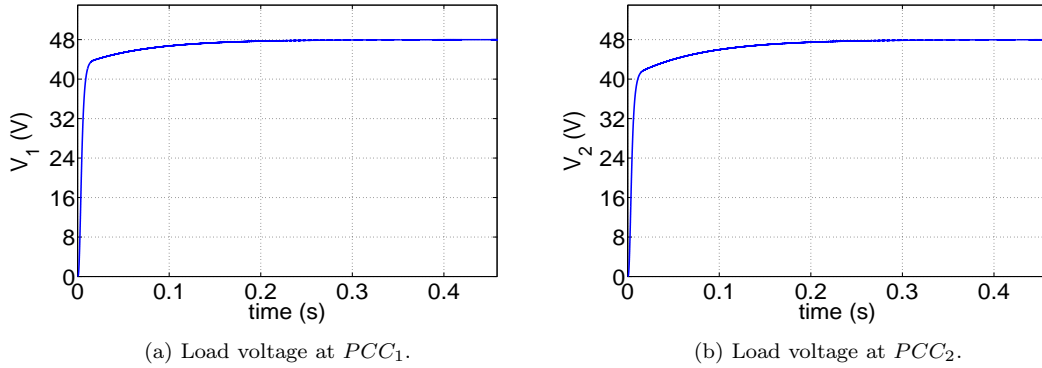


(a) Eigenvalues of the two decoupled closed-loop QSL subsystems. (b) Bode magnitude plot of pre-filters  $\tilde{C}_{[i]}$ ,  $i = 1, 2$ .



(c) Bode magnitude plot of  $F_i(s)$ ,  $i = 1, 2$  with (green) and without (blue) pre-filters.

Figure 5: Features of PnP controllers for Scenario 1 when the DGUs are not interconnected.



(a) Load voltage at  $PCC_1$ .

(b) Load voltage at  $PCC_2$ .

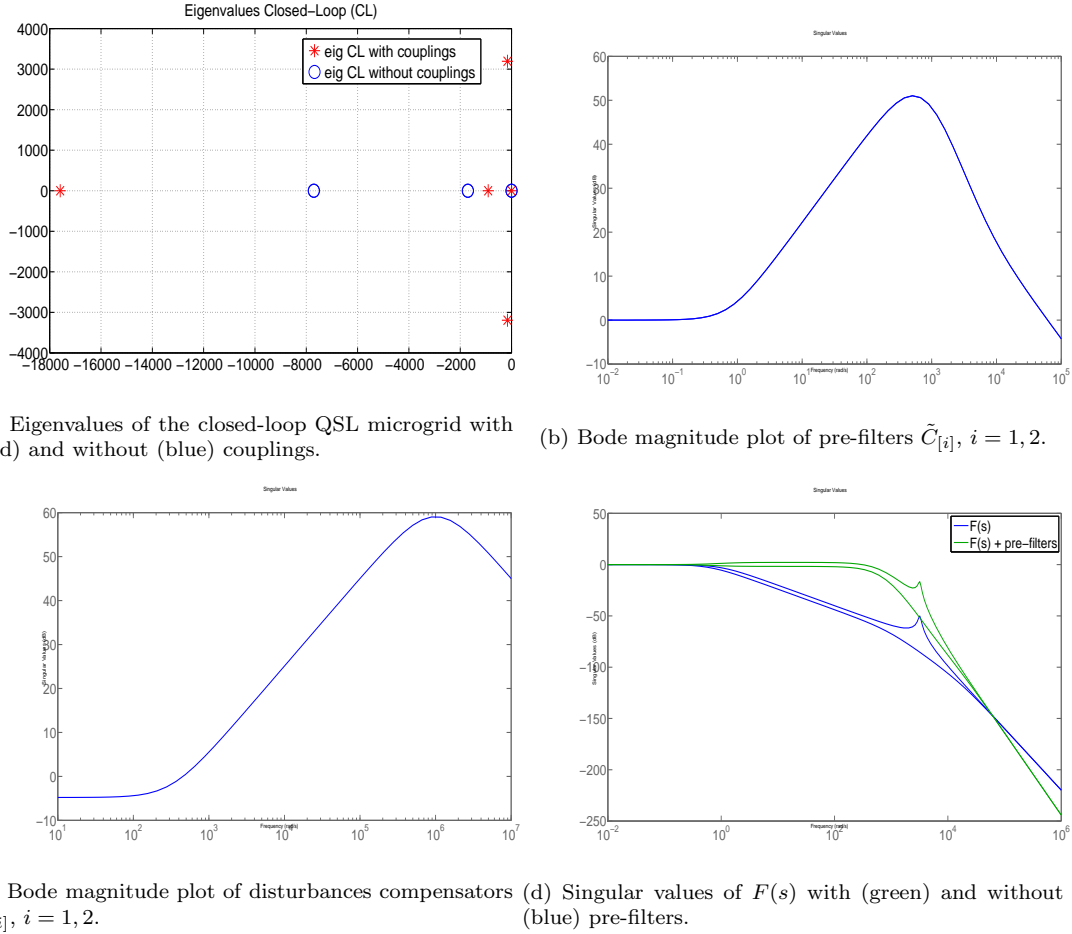
Figure 6: Scenario 1 - Voltage reference tracking at the startup.

#### 4.1.2 Hot plugging-in of DGUs 1 and 2

At time  $t = 2$  s, we connect DGUs 1 and 2 together. This requires real-time switch of the local controllers which translates into two hot plugging-in operations as described in Section 3.5. The new decentralized controllers for subsystems  $\hat{\Sigma}_{[1]}^{DGU}$  and  $\hat{\Sigma}_{[2]}^{DGU}$  are designed running Algorithm 1. Notice that the interconnection of the two subsystems lead to a variation of each DGU dynamics,

therefore even compensators  $\tilde{C}_{[i]}$  and  $N_{[i]}$ ,  $i = 1, 2$  need to be updated. In particular, the new desired closed-loop transfer functions  $\tilde{F}_i(s)$ ,  $i = 1, 2$  have been chosen as low-pass filters with DC gain equal to 0 dB and bandwidth equal to 100 Hz.

Since Algorithm 1 never stops in Step A, the hot plug-in of the DGUs is allowed and local controllers get replaced by the new ones at  $t = 2$  s. Figure 7a shows the closed-loop eigenvalues of the overall QSL ImG composed of two interconnected DGUs. The Bode magnitude plots of compensators  $\tilde{C}_{[i]}$  and  $N_{[i]}$ ,  $i = 1, 2$  are depicted in Figure 7b and 7c, respectively, while the singular values of the overall closed-loop transfer function  $F(s)$  with inputs  $[z_{ref[1]}, z_{ref[2]}]^T$  and outputs  $[z_{[1]}, z_{[2]}]^T$  are shown in Figure 7d.



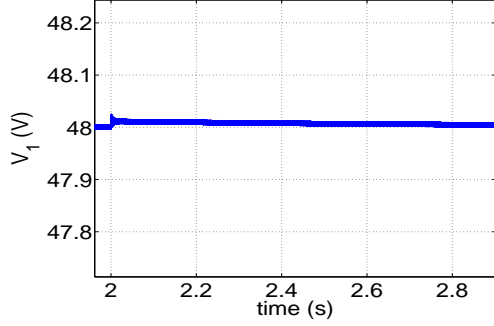
(a) Eigenvalues of the closed-loop QSL microgrid with (red) and without (blue) couplings. (b) Bode magnitude plot of pre-filters  $\tilde{C}_{[i]}$ ,  $i = 1, 2$ . (c) Bode magnitude plot of disturbances compensators  $N_{[i]}$ ,  $i = 1, 2$ . (d) Singular values of  $F(s)$  with (green) and without (blue) pre-filters.

Figure 7: Features of PnP controllers for Scenario 1 when the DGUs are connected together.

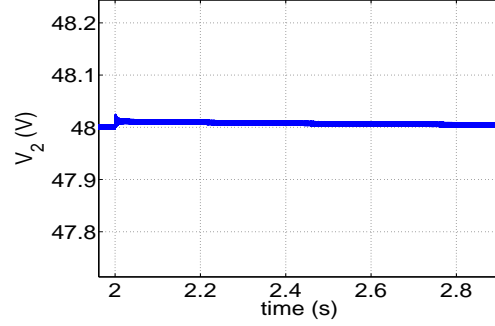
Figure 8 shows the dynamic responses of the voltages at  $PCC_1$  and  $PCC_2$  when the subsystems are connected together. We highlight that the bumpless control transfer schemes ensure no significant deviations in the output signals when the controller switch is performed. Moreover, through the proposed decentralized control strategy, voltage regulation is excellent.

#### 4.1.3 Robustness to unknown load dynamics

Next, we assess the performance of PnP controllers when loads suddenly change at a certain time. To this purpose, at  $t = 3$  s we decrease the load resistances at  $PCC_1$  and  $PCC_2$  to half of their initial values. Figure 9 shows the response of the ImGs. Figures 9a and 9b show the load voltage at  $PCC_1$  and  $PCC_2$  which confirm very good compensation of the current disturbances produced by load changes. We notice small oscillations of the voltage signals due to the presence of complex



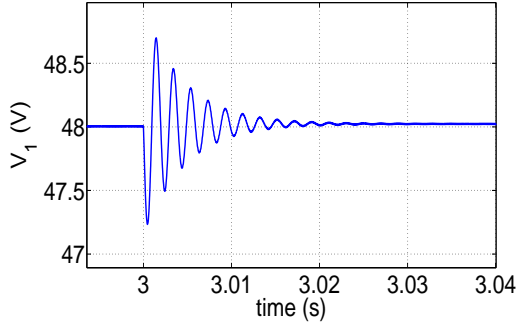
(a) Load voltage at  $PCC_1$ .



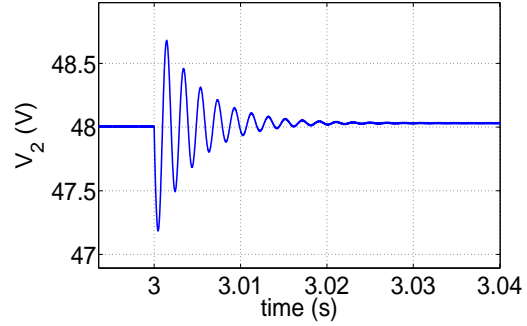
(b) Load voltage at  $PCC_2$ .

Figure 8: Scenario 1 - Impact of bumpless control transfer on the hot plug-in at time  $t = 2$  s.

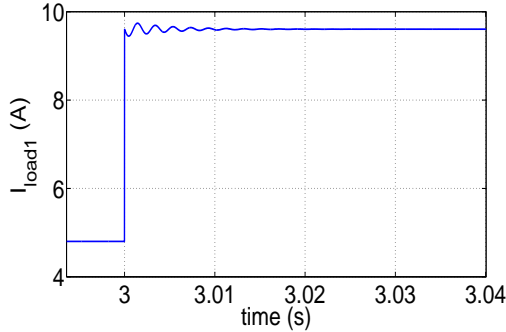
conjugate poles in the transfer function of the closed-loop overall system including couplings (as shown in Figure 7a). However, these oscillations disappear after a short transient. We recall that load currents (see Figures 9c and 9d) are treated as measurable disturbances in our model. Varying the load resistance, induces step-like changes in the disturbances.



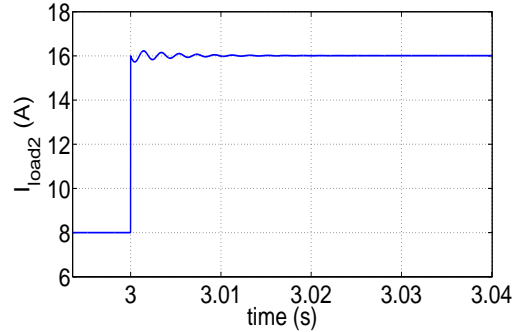
(a) Voltage at  $PCC_1$ .



(b) Voltage at  $PCC_2$ .



(c) Instantaneous load current  $I_{L1}$ .



(d) Instantaneous load current  $I_{L2}$ .

Figure 9: Scenario 1 - Performance of PnP decentralized voltage control in presence of load switches at time  $t = 3$  s.

#### 4.1.4 Voltage tracking for DGU 1

Finally, we evaluate the performance in tracking step changes in the voltage reference at one  $PCC$  (e.g.  $PCC_1$ ) when the DGUs are connected together. This test is of particular concern if we



look at the concrete implementation of islanded DC microgrids. In fact, changes in the voltage references can be required in order to regulate power flow among the DGUs, or to control the state-of-charge of possible batteries embedded in the ImG.

To this purpose, at  $t = 4$  s we let the reference signal of DGU 1,  $v_{1, MG}^*$ , step down to 47.6 V. Notice that this small variation of the voltage reference at  $PCC_1$  is sufficient to let an appreciable amount of current flow through the line, since the line impedance is quite small. The dynamic responses of the overall microgrid to this change are shown in Figure 10. As one can see, controllers guarantees good tracking performances in a reasonable time with small interactions between the two DGUs.

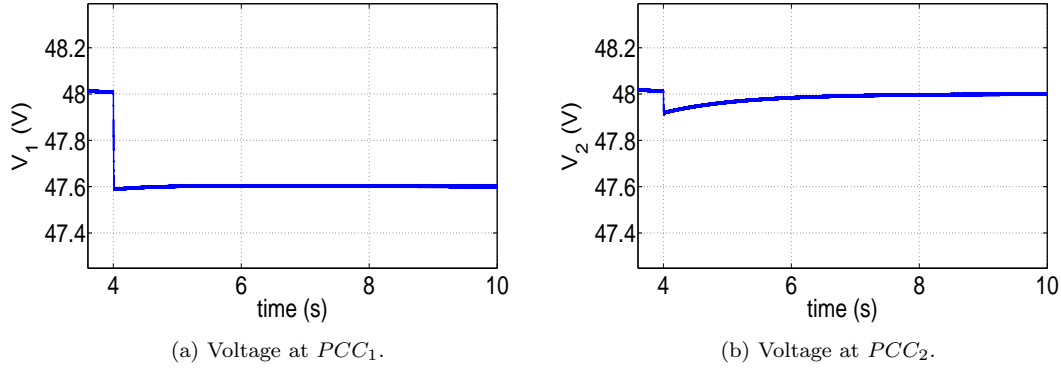


Figure 10: Scenario 1 - Performance of PnP decentralized voltage controllers in terms of set-point tracking for DGU 1.

## 4.2 Scenario 2

In this second scenario, we consider the meshed ImG shown in Figure 11. As one can notice, the main difference with respect to Scenario 1 is that some DGUs have more than one neighbour. This means that the disturbances influencing their dynamics will be greater. Moreover, the presence of a loop further complicates voltage regulation. To our knowledge, control of loop-interconnected DGUs has never been investigated for DC microgrids.

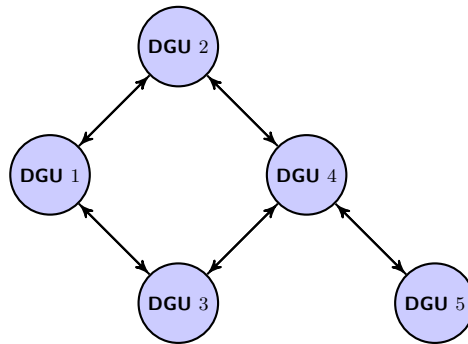
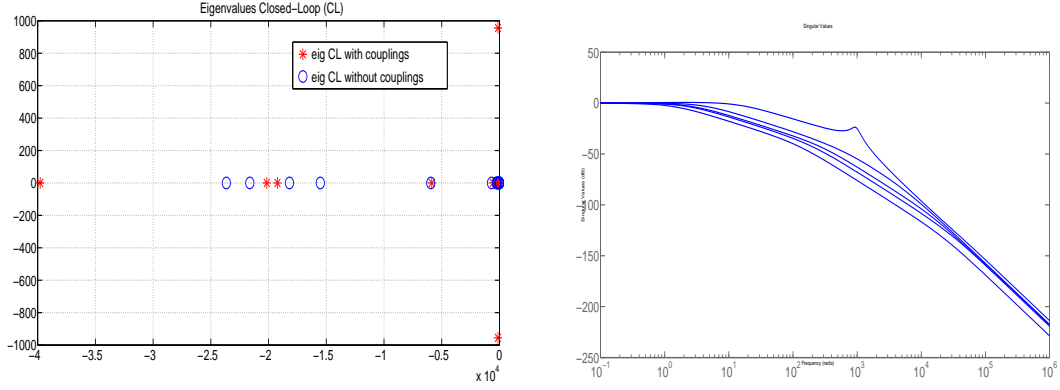


Figure 11: Scenario 2 - Scheme of the ImG composed of 5 DGUs, connected through transmission lines (black arrows).

In order to assess the capability of the proposed decentralized approach to cope with heterogeneous dynamics, we consider an ImG composed of DGUs with non-identical electrical parameters. They are listed in Tables 2, 3 and 4 in Appendix C.

We also assume that DGUs 1-5 supply 10  $\Omega$ , 6  $\Omega$ , 20  $\Omega$ , 2  $\Omega$  and 4  $\Omega$  loads, respectively. Moreover, we highlight that, for this Scenario, no compensators  $\tilde{C}_i$  and  $N_i$  have been used. At the

beginning of the simulation, all the DGUs are assumed to be isolated and not connected to each other. However, we choose to equip each subsystem  $\hat{\Sigma}_{[i]}^{DGU}$ ,  $i \in \mathcal{D} = \{1, \dots, 5\}$ , with controllers  $\mathcal{C}_{[i]}$  designed by running Algorithm 1 and taking into account couplings among DGUs. This is possible because, as shown in Section 3.2, local controllers stabilize the ImG also in absence of couplings. Because of this choice of local controllers in the startup phase, when the five subsystems are connected together at time  $t = 1.5$  s, no bumpless control scheme is required since no real-time switch of controllers is performed. The closed-loop eigenvalues of the overall QSL ImG are depicted in Figure 12a while Figure 12b shows the closed-loop transfer function of the whole microgrid.



(a) Eigenvalues of the closed-loop QSL microgrid with (red) and without (blue) couplings.

(b) Singular values of  $F(s)$ .

Figure 12: Features of PnP controllers for Scenario 2 with 5 interconnected DGUs.

#### 4.2.1 Plug-in of a new DGU

For evaluating the PnP capabilities of our control approach, we simulate the connection of DGU  $\hat{\Sigma}_{[6]}^{DGU}$  with  $\hat{\Sigma}_{[1]}^{DGU}$  and  $\hat{\Sigma}_{[5]}^{DGU}$ , as shown in Figure 13. Therefore, we have  $\mathcal{N}_6 = \{1, 5\}$ . In

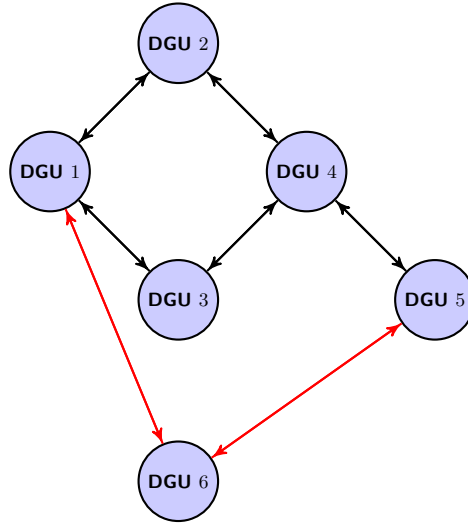


Figure 13: Scenario 2 - Scheme of the ImG composed of 6 DGUs after the plugging-in of  $\hat{\Sigma}_{[6]}^{DGU}$ .

principle, subsystems  $\hat{\Sigma}_{[j]}^{DGU}$ ,  $j \in \mathcal{N}_6$  must update their controllers  $\mathcal{C}_{[j]}$  (see Section 3.5). However, we highlight that previous controllers for DGUs  $\hat{\Sigma}_{[1]}^{DGU}$  and  $\hat{\Sigma}_{[5]}^{DGU}$  can be also maintained, provided

that the already computed matrices  $K_j$ ,  $j \in \mathcal{N}_6$  still fulfill all constraints in (26) for the new ImG topology. Since this test succeeds, we proceed by executing Algorithm 1 for synthesizing  $\mathcal{C}_{[6]}$  for the new DGU only. Algorithm 1 never stops in Step A and therefore the addition of  $\hat{\Sigma}_{[6]}^{DGU}$  is allowed. The real-time plugging-in of  $\hat{\Sigma}_{[6]}^{DGU}$  is executed at time  $t = 2$  s. Until the plug-in of  $\hat{\Sigma}_{[6]}^{DGU}$ , common reference  $v_{MG}^*$  for DGUs 1-5 is the same as for DGUs 1-2 in Scenario 1 and the subsystem  $\hat{\Sigma}_{[6]}^{DGU}$  is assumed to work isolated, tracking the reference voltage  $v_{MG}^*$ . Figures 14a and 14b show respectively the closed-loop eigenvalues and the singular values of the closed-loop  $F(s)$  of the overall QSL ImG in Figure 13 equipped with the controllers described above. From Figure 15, we note that right after the hot plug-in of  $\hat{\Sigma}_{[6]}^{DGU}$  at  $t = 2$  s, load voltages of  $\hat{\Sigma}_{[1]}^{DGU}$  and  $\hat{\Sigma}_{[5]}^{DGU}$  do not deviate from the respective reference signals.

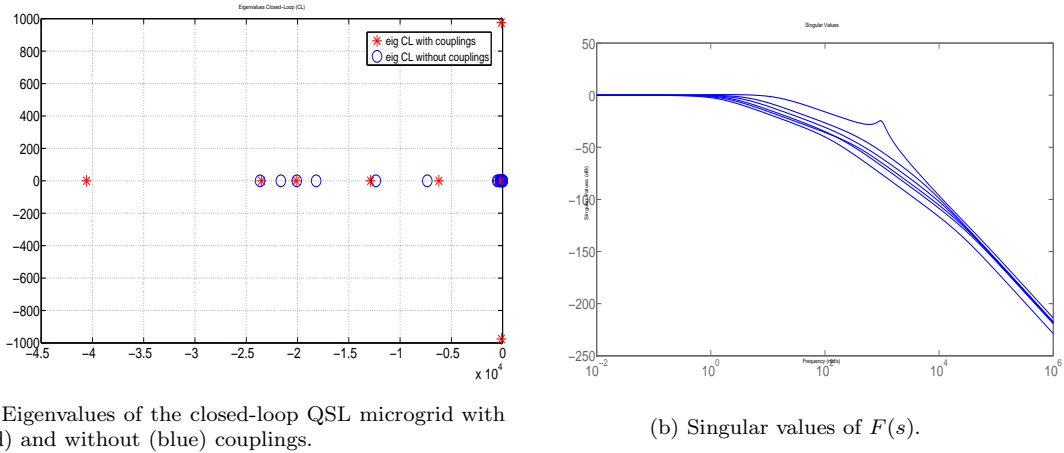


Figure 14: Features of PnP controllers for Scenario 2 with 6 interconnected DGUs

#### 4.2.2 Robustness to unknown load dynamics

In order to test the robustness of the overall ImG to unknown load dynamics, at  $t = 3$  s we halve the load of DGU 6, which was equal to  $8 \Omega$  for  $t < 3$  s.

Figures 16a and 16b show that, when the load change of  $\hat{\Sigma}_{[6]}^{DGU}$  occurs, the voltages at  $PCC_1$  and  $PCC_5$  exhibit very small variations which last for a short time. Then, load voltages of  $\hat{\Sigma}_{[1]}^{DGU}$  and  $\hat{\Sigma}_{[5]}^{DGU}$  converge to their reference values. Similar remarks can be done for the new DGU  $\hat{\Sigma}_{[6]}^{DGU}$ : as shown in Figure 16c, there is a short transient at the time of the load change, that is effectively compensated by the control action. These experiments highlight that controllers  $\mathcal{C}_{[i]}$ ,  $i = 1, \dots, 6$  may ensure very good tracking of the reference signal and robustness to unknown load dynamics even without using compensators  $\tilde{\mathcal{C}}_{[6]}$  and  $N_{[6]}$ .

#### 4.2.3 Unplugging of a DGU

Next, we simulate the disconnection of  $\hat{\Sigma}_{[3]}^{DGU}$  so that the considered ImG assumes the topology shown in Figure 17. The set of neighbours of DGU 3 is  $\mathcal{N}_3 = \{1, 4\}$ .

Because of the disconnection, there is a change in the local dynamics  $\hat{A}_{jj}$  of DGUs  $\hat{\Sigma}_{[j]}^{DGU}$ ,  $j \in \mathcal{N}_3$ . Then, in theory, each controller  $\mathcal{C}_{[j]}$ ,  $j \in \mathcal{N}_3$  must be redesigned (see Section 3.5). As for the plugging-in operation, we decide to maintain the previous controller for DGUs 1 and 4, after checking that the already computed matrices  $K_j$ ,  $j \in \mathcal{N}_3$  fulfill all constraints in (26) even when DGU 3 is removed. Since this test ends successfully, the disconnection of  $\hat{\Sigma}_{[3]}^{DGU}$  is allowed. Figure 18a shows that the closed-loop model of the new QSL microgrid is still asymptotically stable in

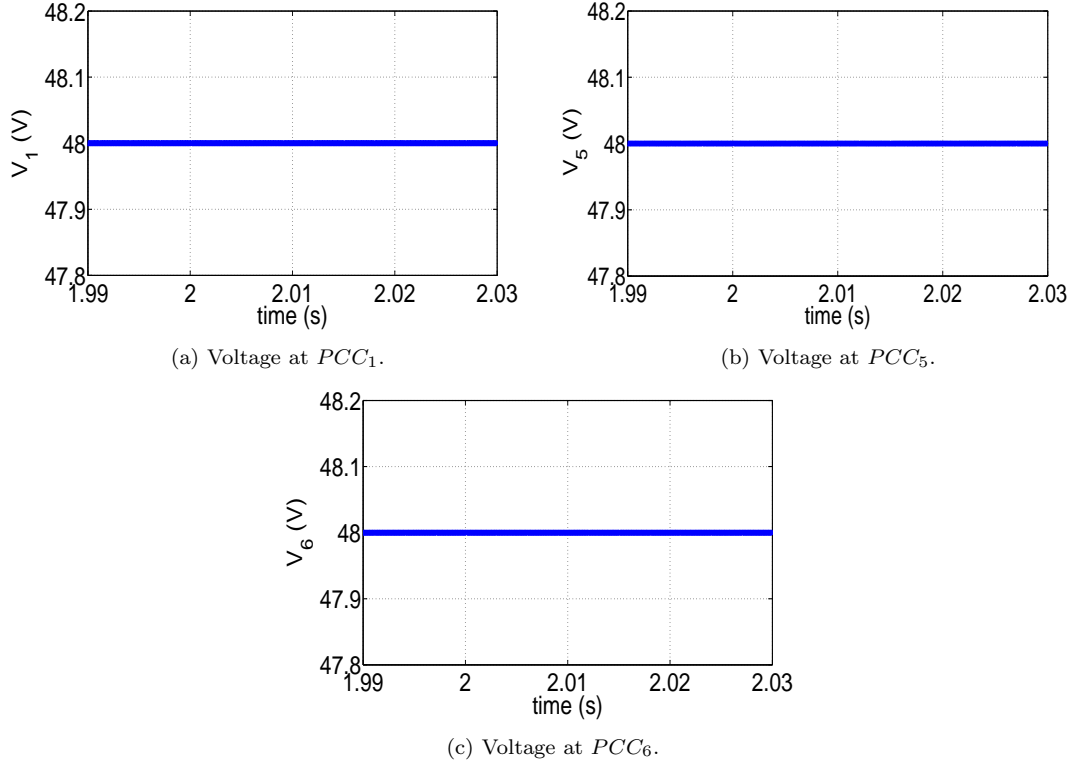


Figure 15: Scenario 2 - Performance of PnP decentralized voltage controllers during the hot plug-in of DGU 6 at time  $t = 2$  s.

spite of the unplugging operation while Figure 18b shows the closed-loop transfer function  $F(s)$  of the ImG. Hot-unplugging of  $\hat{\Sigma}_{[3]}^{DGU}$  is performed at time  $t = 7$  s. As shown in Figure 19, the load voltages of DGU  $\hat{\Sigma}_{[j]}^{DGU}$ ,  $j \in \mathcal{N}_3$  do not deviate from the respective reference signals. We stress again that stability of the microgrid is preserved despite the disconnection of  $\hat{\Sigma}_{[3]}^{DGU}$ .

## 5 Conclusions

In this paper, a decentralized control scheme for guaranteeing voltage stability in DC ImGs was presented. The main feature of the proposed approach is that, whenever a plugging-in or -out of DGUs is required, only a limited number of local controllers must be updated. Moreover, as mentioned in Section 4.1.4, local voltage controllers should be coupled with a higher control layer devoted to power flow regulation so as to orchestrate mutual help among DGUs. To this purpose, we will study if and how ideas from secondary control of ImGs [7] can be reappraised in our context.

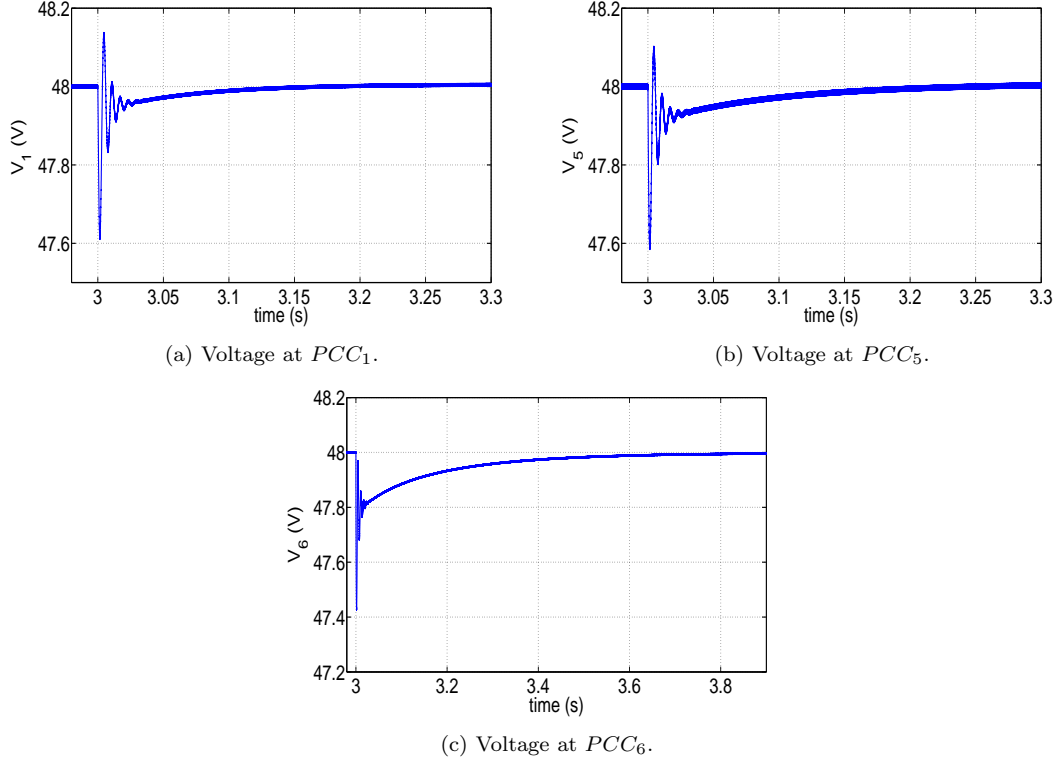


Figure 16: Scenario 2 - Performance of PnP decentralized voltage controllers in terms of robustness to an abrupt change of load resistances at time  $t = 3$  s.

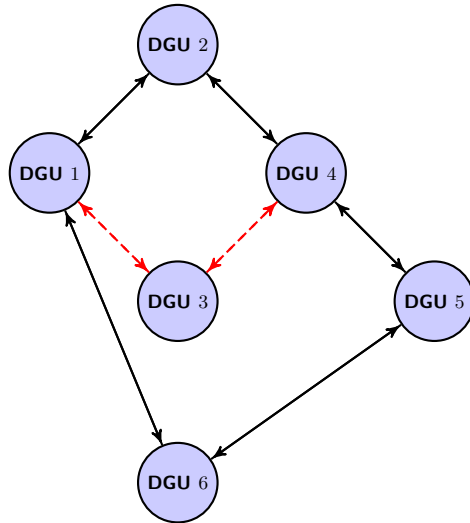
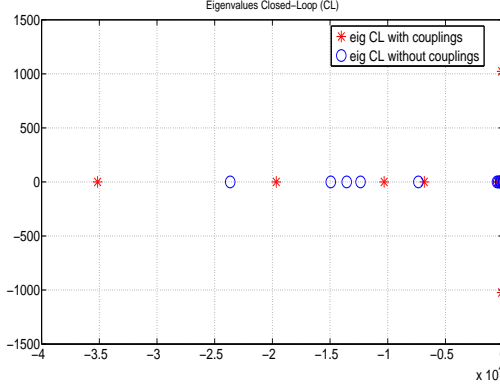
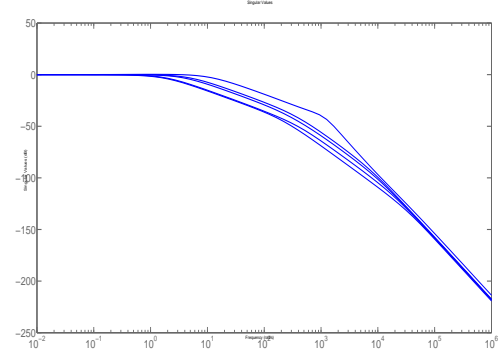


Figure 17: Scenario 2 - Scheme of the ImG composed of 5 DGUs after the unplugging of  $\hat{\Sigma}_{[3]}^{DGU}$ .

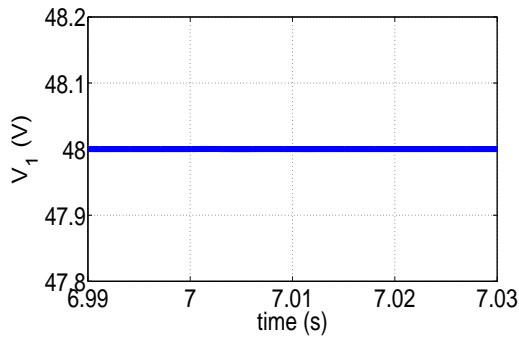


(a) Eigenvalues of the closed-loop QSL microgrid with (red) and without (blue) couplings.

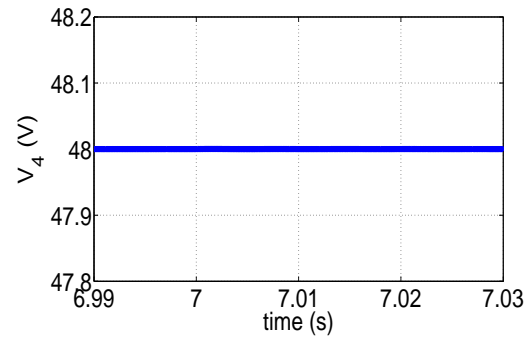


(b) Singular values of  $F(s)$ .

Figure 18: Features of PnP controllers for Scenario 2 after the unplugging of DGU 3.



(a) Voltage at  $PCC_1$ .



(b) Voltage at  $PCC_4$ .

Figure 19: Scenario 2 - Performance of PnP decentralized voltage controllers during the hot-unplugging of DGU 3 at  $t = 7$  s.

## A Matrices appearing in microgrid models

The following appendix collects all matrices appearing in Section 2.

### A.1 Matrices in the model (2)

$$A = \begin{bmatrix} 0 & \frac{1}{C_{ti}} & \frac{1}{C_{ti}} & 0 & 0 & 0 \\ -\frac{1}{L_{ti}} & -\frac{R_{ti}}{L_{ti}} & 0 & 0 & 0 & 0 \\ -\frac{1}{L_{ij}} & 0 & -\frac{R_{ij}}{L_{ij}} & 0 & \frac{1}{L_{ij}} & 0 \\ \frac{1}{L_{ji}} & 0 & 0 & -\frac{R_{ji}}{L_{ji}} & -\frac{1}{L_{ji}} & 0 \\ 0 & 0 & 0 & \frac{1}{C_{tj}} & 0 & \frac{1}{C_{tj}} \\ 0 & 0 & 0 & 0 & -\frac{1}{L_{tj}} & -\frac{R_{tj}}{L_{tj}} \end{bmatrix}$$

$$B = \begin{bmatrix} 0 & 0 \\ \frac{1}{L_{ti}} & 0 \\ 0 & 0 \\ 0 & 0 \\ 0 & 0 \\ 0 & \frac{1}{L_{tj}} \end{bmatrix} \quad C^T = \begin{bmatrix} 1 & 0 \\ 0 & 0 \\ 0 & 0 \\ 0 & 0 \\ 0 & 1 \\ 0 & 0 \end{bmatrix} \quad M = \begin{bmatrix} -\frac{1}{C_{ti}} & 0 \\ 0 & 0 \\ 0 & 0 \\ 0 & 0 \\ 0 & -\frac{1}{C_{tj}} \\ 0 & 0 \end{bmatrix}$$

### A.2 Matrices in the QSL model (5) and (6)

DGU- $i$ ,  $i \in \{1, 2\}$

$$A_{ii} = \begin{bmatrix} -\frac{1}{R_{ij}C_{ti}} & \frac{1}{C_{ti}} \\ -\frac{1}{L_{ti}} & -\frac{R_{ti}}{L_{ti}} \end{bmatrix}$$

$$A_{ij} = \begin{bmatrix} \frac{1}{R_{ij}C_{ti}} & 0 \\ 0 & 0 \end{bmatrix}$$

$$B_i = \begin{bmatrix} 0 \\ \frac{1}{L_{ti}} \end{bmatrix} \quad M_i = \begin{bmatrix} -\frac{1}{C_{ti}} \\ 0 \end{bmatrix} \quad C_i = \begin{bmatrix} 1 & 0 \\ 0 & 1 \end{bmatrix} \quad H_i = \begin{bmatrix} 1 & 0 \end{bmatrix}$$

Line  $i \neq j$

$$A_{li,ij} = \begin{bmatrix} -\frac{1}{L_{ij}} & 0 \end{bmatrix} \quad A_{lj,ij} = \begin{bmatrix} \frac{1}{L_{ij}} & 0 \end{bmatrix} \quad A_{ll,ij} = -\frac{R_{ij}}{L_{ij}} \quad (41)$$

### A.3 QSL model of microgrid composed of $N$ DGUs

DGU- $i$ ,  $i \in \mathcal{D}$

$$A_{ii} = \begin{bmatrix} \sum_{j \in \mathcal{N}_i} -\frac{1}{R_{ij}C_{ti}} & \frac{1}{C_{ti}} \\ -\frac{1}{L_{ti}} & -\frac{R_{ti}}{L_{ti}} \end{bmatrix} \quad (42)$$

$$A_{ij} = \begin{bmatrix} \frac{1}{R_{ij}C_{ti}} & 0 \\ 0 & 0 \end{bmatrix} \quad (43)$$

We remind that  $R_{ij}$  and  $L_{ij}$  are the resistance and the inductance of the line between DGU  $i$  and DGU  $j$ . Moreover, matrices  $B_i$ ,  $C_i$ ,  $M_i$  and  $H_i$  are equal to those appearing in Section A.2.

Overall model of a microgrid composed by  $N$  DGUs

$$\begin{aligned}
\begin{bmatrix} \dot{x}_{[1]} \\ \dot{x}_{[2]} \\ \dot{x}_{[3]} \\ \vdots \\ \dot{x}_{[N]} \end{bmatrix} &= \underbrace{\begin{bmatrix} A_{11} & A_{12} & A_{13} & \dots & A_{1N} \\ A_{21} & A_{22} & A_{23} & \dots & A_{2N} \\ A_{31} & A_{32} & A_{3l} & \dots & A_{3N} \\ \vdots & \vdots & \vdots & \ddots & \vdots \\ A_{N1} & A_{N2} & A_{N3} & \dots & A_{NN} \end{bmatrix}}_{\mathbf{A}} \begin{bmatrix} x_{[1]} \\ x_{[2]} \\ x_{[3]} \\ \vdots \\ x_{[N]} \end{bmatrix} + \\
&+ \underbrace{\begin{bmatrix} B_1 & 0 & \dots & 0 \\ 0 & B_2 & \ddots & \vdots \\ \vdots & \ddots & \ddots & 0 \\ 0 & \dots & 0 & B_N \end{bmatrix}}_{\mathbf{B}} \begin{bmatrix} u_{[1]} \\ u_{[2]} \\ \vdots \\ u_{[N]} \end{bmatrix} + \underbrace{\begin{bmatrix} M_1 & 0 & \dots & 0 \\ 0 & M_2 & \ddots & \vdots \\ \vdots & \ddots & \ddots & 0 \\ 0 & \dots & 0 & M_N \end{bmatrix}}_{\mathbf{M}} \begin{bmatrix} d_{[1]} \\ d_{[2]} \\ \vdots \\ d_{[N]} \end{bmatrix} \\
\begin{bmatrix} y_{[1]} \\ y_{[2]} \\ y_{[3]} \\ \vdots \\ y_{[N]} \end{bmatrix} &= \underbrace{\begin{bmatrix} C_1 & 0 & 0 & \dots & 0 \\ 0 & C_2 & 0 & \ddots & \vdots \\ 0 & 0 & C_3 & \ddots & 0 \\ \vdots & \ddots & \ddots & \ddots & 0 \\ 0 & \dots & 0 & 0 & C_N \end{bmatrix}}_{\mathbf{C}} \begin{bmatrix} x_{[1]} \\ x_{[2]} \\ x_{[3]} \\ \vdots \\ x_{[N]} \end{bmatrix} \\
\begin{bmatrix} z_{[1]} \\ z_{[2]} \\ z_{[3]} \\ \vdots \\ z_{[N]} \end{bmatrix} &= \underbrace{\begin{bmatrix} H_1 & 0 & 0 & \dots & 0 \\ 0 & H_2 & 0 & \ddots & \vdots \\ 0 & 0 & H_3 & \ddots & 0 \\ \vdots & \ddots & \ddots & \ddots & 0 \\ 0 & \dots & 0 & 0 & H_N \end{bmatrix}}_{\mathbf{H}} \begin{bmatrix} y_{[1]} \\ y_{[2]} \\ y_{[3]} \\ \vdots \\ y_{[N]} \end{bmatrix}.
\end{aligned} \tag{44}$$



## B Bumpless control transfer

Since the controller is a dynamic system, it is necessary to make sure that the state of the system is correct when a switch of the controller (i.e. a plugging-in or unplugging operation) is required. Assuming that the control switch is made at a certain point in time  $\bar{t}$ , we call  $u_{prec,i}$  the control signal produced by the controller  $\mathcal{C}_i$  up to time  $\bar{t}$ . It might happen that the updated controller will provide a control variable  $u_i$  different from  $u_{prec,i}$ . Therefore, it is necessary to ensure there is no substantial change in the two outputs at  $\bar{t}$ . This is called *bumpless control transfer* [18].

A bumpless control transfer implementation of PnP local controller for system  $\hat{\Sigma}_i^{DGU}$  is illustrated in Figure 20.

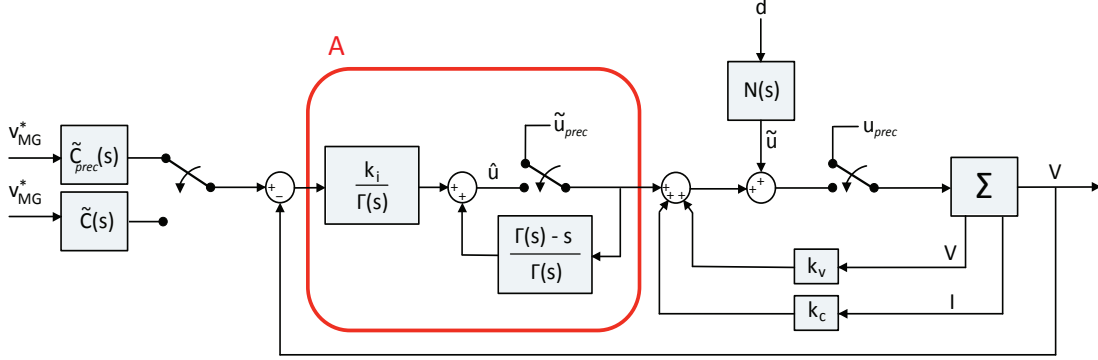


Figure 20: Bumpless control transfer implementation.

For the sake of simplicity we drop here the index  $i$  of the subsystem and associated local variables and all switches in Figure 20 are assumed to commute at time  $\bar{t}$ . In the Figure, vector

$$K = [k_v \ k_c \ k_i]^T$$

contains the parameters of the local controller to be activated at time  $\bar{t}$ . Notice that the integrator embedded in the DGU model for zeroing the steady-state error is replaced by block A (highlighted in red in Figure 20), where the polynomial  $\Gamma(s)$  has to be chosen such that  $k_i > \Gamma(0)$  and the transfer function

$$\Psi = \frac{\Gamma(s) - s}{\Gamma(s)}$$

is asymptotically stable and realizable. In block A, a switch is present so that the signal is either  $\tilde{u}_{prec}$  (up to time  $\bar{t}$ ) or  $\hat{u}$  (right after  $\bar{t}$ ). The variable  $\tilde{u}_{prec}$  is given by

$$\tilde{u}_{prec} = u_{prec} - k_v V - k_c I_t - \tilde{u} \quad (45)$$

where  $\tilde{u}$  is the additional input produced by compensator  $N(s)$ , computed with respect to the dynamics of the system after the commutation (set  $N(s) = 0$  if such a compensation is not implemented). We highlight that since there could be a transient in the  $\hat{u}$  response to track signal  $\tilde{u}_{prec}$ , it is fundamental to wait for the two signals to become similar before proceeding with the commutation. In this way we avoid jumps in the control variable.

Furthermore, if an optional prefilter of the reference is implemented, at time  $\bar{t}$  is also necessary to commute from transfer function  $\tilde{C}_{prec}(s)$  to  $\tilde{C}(s)$ , since each plugging-in or unplugging operation of other DGUs in the overall ImG lead to a variation of the local dynamics of the considered subsystem  $\hat{\Sigma}_i^{DGU}$  (see the term  $\sum_{j \in \mathcal{N}_i} -\frac{1}{R_{ij}C_{ti}}$  in (42)).

## C Electrical and simulation parameters of Scenario 1 and 2

In this appendix, we provide all the electrical and simulation parameters of Scenarios 1 and 2 (which are described in Sections 4.1 and 4.2, respectively).

Parameter	Symbol	Value
DC power supply	$V_{DC}$	100 V
Output capacitance	$C_{t*}$	2.2 mF
Converter inductance	$L_{t*}$	1.8 mH
Inductor + switch loss resistance	$R_{t*}$	0.2 $\Omega$
Switching frequency	$f_{sw}$	10 kHz
Transmission line inductance	$L_{*o}$	1.8 $\mu H$
Transmission line resistance	$R_{*o}$	0.05 $\Omega$

Table 1: Electrical setup and line parameters

Table 2: VSC filter parameters for DGUs  $\hat{\Sigma}_{[i]}^{DGU}$ ,  $i = \{1, \dots, 6\}$  in Scenario 2.

DGU	Resistance $R_t(\Omega)$	Capacitance $C_t(mF)$	Inductance $L_t(mH)$
$\hat{\Sigma}_{[1]}^{DGU}$	0.2	2.2	1.8
$\hat{\Sigma}_{[2]}^{DGU}$	0.3	1.9	2.0
$\hat{\Sigma}_{[3]}^{DGU}$	0.1	1.7	2.2
$\hat{\Sigma}_{[4]}^{DGU}$	0.5	2.5	3.0
$\hat{\Sigma}_{[5]}^{DGU}$	0.4	2.0	1.2
$\hat{\Sigma}_{[6]}^{DGU}$	0.6	3.0	2.5

Table 3: Transmission lines parameters for Scenario 2.

Connected DGUs ( $i, j$ )	Resistance $R_s(\Omega)$	Inductance $L_s(\mu H)$
(1, 2)	0.05	2.1
(1, 3)	0.07	1.8
(3, 4)	0.06	1.0
(2, 4)	0.04	2.3
(4, 5)	0.08	1.8
(1, 6)	0.1	2.5
(5, 6)	0.08	3.0

Table 4: Common parameters of DGUs  $\hat{\Sigma}_{[i]}^{DGU}$ ,  $i = \{1, \dots, 6\}$  in Scenario 2.

Parameter	Symbol	Value
Electrical parameters		
DC power supply	$V_{DC}$	100 $V$
Output capacitance	$C_t$	2.2 $mF$
Converter inductance	$L_t$	1.8 $mH$
Inductor+switch loss resistance	$R_t$	0.2 $\Omega$
Switching frequency	$f_{sw}$	10 kHz

## References

- [1] R. Lasseter, A. Akhil, C. Marnay, J. Stephens, J. Dagle, R. Guttromson, A. Meliopoulos, R. Yinger, and J. Eto, “The certs microgrid concept,” *White paper for Transmission Reliability Program, Office of Power Technologies, US Department of Energy*, 2002.
- [2] J. M. Guerrero, M. Chandorkar, T.-L. Lee, and P. C. Loh, “Advanced control architectures for intelligent microgrids - part I: decentralized and hierarchical control,” *IEEE Transactions on Industrial Electronics*, vol. 60, no. 4, pp. 1254–1262, 2013.
- [3] J. M. Guerrero, P. C. Loh, T.-L. Lee, and M. Chandorkar, “Advanced control architectures for intelligent microgrids - part II: Power quality, energy storage, and ac/dc microgrids,” *IEEE Transactions on Industrial Electronics*, vol. 60, no. 4, pp. 1263–1270, 2013.
- [4] S. Rivero, F. Sarzo, and G. Ferrari-Trecate, “Plug-and-play voltage and frequency control of islanded microgrids with meshed topology,” *IEEE Transactions on Smart Grid*, 2014. [Online]. Available: doi={10.1109/TSG.2014.2381093}
- [5] —, “Plug-and-play voltage and frequency control of islanded microgrids with meshed topology,” Dipartimento di Ingegneria Industriale e dell’Informazione, Università degli Studi di Pavia, Pavia, Italy, Tech. Rep., 2014. [Online]. Available: arXiv:1405.2421
- [6] A. Kwasinski, “Quantitative evaluation of dc microgrids availability: Effects of system architecture and converter topology design choices,” *IEEE Transactions on Power Electronics*, vol. 26, no. 3, pp. 835–851, 2011.
- [7] Q. Shafiee, T. Dragičević, J. C. Vasquez, and J. M. Guerrero, “Hierarchical Control for Multiple DC-Microgrids Clusters,” *IEEE Transactions on Energy Conversion*, vol. 29, no. 4, pp. 922–933, 2014.
- [8] A. T. Elsayed, A. A. Mohamed, and O. A. Mohammed, “Dc microgrids and distribution systems: An overview,” *Electric Power Systems Research*, vol. 119, pp. 407–417, 2015.
- [9] J. W. Simpson-Porco, F. Dörfler, and F. Bullo, “Synchronization and power sharing for droop-controlled inverters in islanded microgrids,” *Automatica*, vol. 49, no. 9, pp. 2603–2611, 2013.
- [10] A. H. Etemadi, E. J. Davison, and R. Iravani, “A decentralized robust control strategy for multi-dc microgrids part I: Fundamental concepts,” *IEEE Transactions on Power Delivery*, vol. 27, no. 4, pp. 1843–1853, 2012.
- [11] S. Rivero, M. Farina, and G. Ferrari-Trecate, “Plug-and-Play Decentralized Model Predictive Control for Linear Systems,” *IEEE Transactions on Automatic Control*, vol. 58, no. 10, pp. 2608–2614, 2013.
- [12] —, “Plug-and-Play Model Predictive Control based on robust control invariant sets,” *Automatica*, vol. 50, no. 8, pp. 2179–2186, 2014.
- [13] S. Rivero, “Distributed and plug-and-play control for constrained systems,” Ph.D. dissertation, Università degli Studi di Pavia, 2014. [Online]. Available: [http://sisdin.unipv.it/pnpmpc/phpinclude/papers/phd\\\_thesis\\\_rivero.pdf](http://sisdin.unipv.it/pnpmpc/phpinclude/papers/phd\_thesis\_rivero.pdf)
- [14] J. Stoustrup, “Plug & play control: Control technology towards new challenges,” *European Journal of Control*, vol. 15, no. 3, pp. 311–330, 2009.
- [15] X. Lu, J. M. Guerrero, K. Sun, and J. C. Vasquez, “An improved droop control method for dc microgrids based on low bandwidth communication with dc bus voltage restoration and enhanced current sharing accuracy,” *IEEE Transactions on Power Electronics*, vol. 29, no. 4, pp. 1800–1812, 2014.

- [16] V. Venkatasubramanian, H. Schattler, and J. Zaborszky, “Fast Time-Varying Phasor Analysis in the Balanced Three-Phase Large Electric Power System,” *IEEE Transactions on Automatic Control*, vol. 40, no. 11, pp. 1975–1982, 1995.
- [17] Q. Shafiee, T. Dragičević, J. C. Vasquez, and J. M. Guerrero, “Modeling, Stability Analysis and Active Stabilization of Multiple DC-Microgrid Clusters,” in *Proceedings of the IEEE International Energy Conference (ENERGYCON)*, Dubrovnik, Croatia, May 13-16, 2014, pp. 1284–1290.
- [18] K. J. Åström and T. Hägglund, *Advanced PID control*. ISA-The Instrumentation, Systems, and Automation Society; Research Triangle Park, NC 27709, 2006.
- [19] M. Babazadeh and H. Karimi, “A Robust Two-Degree-of-Freedom Control Strategy for an Islanded Microgrid,” *IEEE Transactions on Power Delivery*, vol. 28, no. 3, pp. 1339–1347, 2013.
- [20] J. Lunze, *Feedback control of large scale systems*. Upper Saddle River, NJ, USA: Prentice Hall, Systems and Control Engineering, 1992.
- [21] H. Akagi, E. H. Watanabe, and M. Aredes, *Instantaneous power theory and applications to power conditioning*. Hoboken, New Jersey, USA: John Wiley & Sons, IEEE Press series on Power Engineering, 2007.
- [22] S. Skogestad and I. Postlethwaite, *Multivariable feedback control: analysis and design*. New York, NY, USA: John Wiley & Sons, 1996.
- [23] S. Boyd, L. El Ghaoui, E. Feron, and V. Balakrishnan, *Linear matrix inequalities in system and control theory*. Philadelphia, Pennsylvania, USA: SIAM Studies in Applied Mathematics, vol. 15, 1994.